



HAL
open science

Protein synthesis increases with photosynthesis via the stimulation of translation initiation

Guillaume Tcherkez, Adam Carroll, Cyril Abadie, Samuel Mainguet, Marlene Davanture, Michel Zivy

► **To cite this version:**

Guillaume Tcherkez, Adam Carroll, Cyril Abadie, Samuel Mainguet, Marlene Davanture, et al.. Protein synthesis increases with photosynthesis via the stimulation of translation initiation. *Plant Science*, 2020, 291, pp.110352. 10.1016/j.plantsci.2019.110352 . hal-02499231

HAL Id: hal-02499231

<https://univ-angers.hal.science/hal-02499231>

Submitted on 17 Nov 2020

HAL is a multi-disciplinary open access archive for the deposit and dissemination of scientific research documents, whether they are published or not. The documents may come from teaching and research institutions in France or abroad, or from public or private research centers.

L'archive ouverte pluridisciplinaire **HAL**, est destinée au dépôt et à la diffusion de documents scientifiques de niveau recherche, publiés ou non, émanant des établissements d'enseignement et de recherche français ou étrangers, des laboratoires publics ou privés.

Corresponding author:

Guillaume Tcherkez
Research School of Biology
ANU Joint College of Sciences
Australian National University
2601 Canberra ACT, Australia
Tel. +61 (0)2 6125 0381
guillaume.tcherkez@anu.edu.au

Protein synthesis increases with photosynthesis via the stimulation of translation initiation

Guillaume Tcherkez^{1,2*}, Adam Carroll³, Cyril Abadie², Samuel Mainguet⁴, Marlène Davanture⁵ and Michel Zivy⁵

1. Research School of Biology, ANU Joint College of Sciences, Australian National University, 2601 Canberra ACT, Australia.

2. Institut de Recherche en Horticulture et Semences, INRA, Université d'Angers, 42 rue Georges Morel, 49070 Beaucouzé, France.

3. Joint Mass Spectrometry Facility, Research School of Chemistry, Australian National University, 2601 Canberra ACT, Australia.

4. Institute of Plant Sciences of Saclay, INRA, University Paris-Sud, CNRS, Université Paris-Saclay, Ferme du Moulon, 91190 Gif-sur-Yvette, France.

5. Plateforme d'Analyse de Protéomique Paris Sud-Ouest (PAPPSO), GQE Le Moulon, INRA, Univ. Paris-Sud, CNRS, AgroParisTech, Université Paris-Saclay, Ferme du Moulon, 91190 Gif-sur-Yvette, France.

*Contact author to whom correspondence should be addressed: Tel. +61 (0)2 6125 0381. E-mail. guillaume.tcherkez@anu.edu.au

Keywords: photosynthesis, photorespiration, protein synthesis, translation, phosphorylation

Number of figures: 4

Number of tables: 1

Word count (w/o abstract, acknowledgements and references): 5,205

Twitter accounts: @ANUmedia; @IRHS_Seed_lab

ORCID numbers:

Guillaume Tcherkez: 0000-0002-3339-956X

1 **Abstract (198 words)**
2

3 Leaf protein synthesis is an essential process at the heart of plant nitrogen (N) homeostasis and
4 turnover that **preferentially** takes place in the light, that is, when N and CO₂ fixation occur. The
5 carbon allocation to protein synthesis in illuminated leaves generally accounts for *ca.* 1% of net
6 photosynthesis. It is likely that protein synthesis activity varies with photosynthetic conditions
7 (CO₂/O₂ atmosphere composition) since changes in photorespiration and carbon provision
8 should in principle impact on amino acid supply as well as metabolic regulation via leaf sugar
9 content. However, possible changes in protein synthesis and translation activity when gaseous
10 conditions vary are virtually unknown. Here, we address this question using metabolomics,
11 isotopic techniques, phosphoproteomics and polysome quantitation, under different
12 photosynthetic conditions that were varied with atmospheric CO₂ and O₂ mole fraction, using
13 illuminated *Arabidopsis* rosettes under controlled gas exchange conditions. We show that
14 carbon allocation to proteins is within 1–2.5% of net photosynthesis, increases with
15 photosynthesis rate and is unrelated to total amino acid **content**. In addition, photosynthesis
16 correlates to polysome abundance and phosphorylation of ribosomal proteins and translation
17 initiation factors. Our results demonstrate that translation activity follows photosynthetic
18 activity, showing the considerable impact of metabolism (carboxylation–oxygenation balance)
19 on protein synthesis.
20

21 1. Introduction

22 It is now nearly 250 years since proteins were extracted and purified from green leaves for the
23 first time [1] and nearly 85 years since protein synthesis (and degradation) activity by leaves
24 was first shown [2-4]. Yet, physiological mechanisms that dictate leaf protein content are
25 presently incompletely understood, and this represents a hurdle in the understanding of leaf
26 primary carbon and nitrogen (N) metabolism. In fact, a considerable proportion of leaf proteins
27 is made of ribulose 1,5-bisphosphate carboxylase/oxygenase (Rubisco) and carbonic anhydrase
28 and is thus directly involved in photosynthetic CO₂ assimilation. The turnover of leaf proteins
29 is the cornerstone of N metabolism, since proteins such as Rubisco are remobilized and used as
30 a N (and sulphur) reservoir during grain filling, fruit development and leaf senescence. Also,
31 protein degradation is regulated by N availability, environmental and internal signals, allowing
32 optimal plant N partitioning and growth [5]. However, relatively little is known about the fast
33 control of protein synthesis in response to common situations in leaves (such as varying CO₂),
34 in contrast with seedlings and roots in which the control of translation under hypoxia has been
35 well-studied. In other words, the regulation of leaf protein synthesis and turnover in the short-
36 term is much less understood.

37
38 It has been shown that there is a diurnal cycle of protein synthesis activity, with higher
39 translation activity (and higher polysome abundance) in the light compared with the dark [6-9].
40 Also, protein synthesis has been suggested to relate to growth rate [10] and sucrose content in
41 the dark [7]. In addition, the effect of light as compared to the dark has been shown to correlate
42 with the phosphorylation of translation initiation factors (eIFs) and ribosomal proteins (such as
43 RPS6), indicating that the control of cytosolic translation initiation plays an important role in
44 circadian (dark/light) protein synthesis regulation [11-14]. Accordingly, pioneering works
45 using isotopic labelling (with ¹⁵N) demonstrated that leaf protein synthesis took place in the
46 light (from nitrate) and was negligible in darkness [15].

47
48 In principle, the photosynthetic rate itself (and therefore, atmospheric gaseous
49 composition) can be anticipated to have an effect on protein synthesis and translation activity.
50 In particular, translation initiation involves several molecular actors that can be associated with
51 metabolic regulation. Briefly, translation initiation starts with the formation of a 43S
52 preinitiation complex, which contains the 40S ribosome subunit and eIFs 5, 3, 1 and 1A. **The**
53 **preinitiation complex binds the eIF2 complex and then the mRNA-eIF(iso)4F complex (here,**
54 **parentheses mean two complexes, eIF4F and eIFiso4F). The plant-specific eIFiso4F complex**
55 **comprises eIFs 4A, 4B, iso4G, iso4E and poly-A binding proteins.** After mRNA scanning and
56 start codon identification, some eIFs are liberated, the ribosomal 60S subunit binds and
57 elongation starts [12, 16].

58
59 Many eIFs or ribosomal proteins (RPs) can be modified post-translationally (in
60 particular, by phosphorylation) and this modulates their activity [17]. **In yeast,** General Control
61 Non-derepressible 2 (GCN2) can phosphorylate eIF2 α under specific nutrient or redox
62 conditions [see, e.g., [18]], preventing guanyl nucleotide recycling. Also, metabolic conditions
63 (sugar and free amino acid content) can impact on the mammalian target of rapamycin (mTOR)
64 signaling pathway which controls RPS6 phosphorylation (for a recent experimental study **in**
65 **Arabidopsis,** see [19]) as well as the sugar-sensing kinase SnRK1 which can phosphorylate
66 eIF(iso)4E [20]. Therefore, it has been hypothesized that photosynthetic activity promotes
67 phosphorylation of RPS6 (amongst other RPs) and the initiation factor eIF4B, and disfavor
68 phosphorylation of eIF2 α , thus stimulating protein synthesis [11]. Furthermore, CO₂ and O₂
69 mole fractions dictate the rate of photorespiration, which could also impact on translation. On
70 the one hand, photorespiration leads to peroxisomal H₂O₂ generation and can induce **oxidative**
71 **stress and perhaps, this might trigger phosphorylation of eIF2 α** [21] thereby inhibiting

72 translation initiation. However, on the other hand, photorespiration produces amino acids
73 (glycine, serine), leads to mitochondrial ATP generation and enhance N assimilation, and this
74 might be accompanied by an increased protein synthesis. Nevertheless, it should be noted that
75 the specific role of GCN proteins is still unclear, and other kinases (such as casein kinase 2,
76 CK2) are capable of phosphorylating eIF2 α *in vitro* [12, 22-25]. Also, an important role of
77 SnRK1 (also involved in sucrose signaling) has been recently shown for eIF4(iso)4G
78 phosphorylation in response to submergence [26].

79 Up to now, there is limited information on the rate of protein synthesis when
80 photosynthesis varies, typically when CO₂ and/or O₂ mole fraction changes. The use of ¹⁵N
81 labelling in barley leaves has suggested that protein synthesis correlated with chlorophyll
82 content and thus potentially with photosynthesis [27]. Also, ¹⁵N labelling in proteins has been
83 found to be much larger with CO₂ in air compared to CO₂-free air, suggesting a coupling with
84 photosynthesis [15]. In photosynthesizing leaves, isotopic pulse labelling (with ¹⁴CO₂) has
85 demonstrated that protein synthesis represents a carbon flux of about 0.1 $\mu\text{mol m}^{-2} \text{s}^{-1}$ and after
86 sugar export has taken place (i.e. after several hours in darkness), ¹⁴C-labelled proteins can
87 represent up to 20% of total leaf radioactivity [28-31] – such a proportion being changed by the
88 presence of close sink organs [32] and leaf age [28]. When photosynthesis with ¹⁴CO₂ was
89 augmented via incident light intensity, proteins represented a lower percentage of total leaf
90 radioactivity but in absolute terms, represented more labelled carbon, with a ¹⁴C-flux of ≈ 0.1
91 $\mu\text{mol m}^{-2} \text{s}^{-1}$ at low light and $\approx 0.25 \mu\text{mol m}^{-2} \text{s}^{-1}$ at high light [33]. In a previous study, we
92 observed that the phosphorylation of some eIFs and RPs could respond to CO₂ mole fraction,
93 suggesting there is an increase of translation activity when photosynthesis increases [11].

94 However, there is presently no specific study exploring and quantifying the impact of
95 photosynthetic conditions on leaf protein synthesis and in particular, the short-term effect of
96 CO₂ and O₂ mole fraction (and thus the balance between gross photosynthesis and
97 photorespiration). This lack of knowledge is problematic because the turnover rate of proteins
98 may affect not only N assimilation but also photosynthetic capacity itself. In fact, while it is
99 rather unlikely that the very high Rubisco content changes dramatically in the short-term when
100 photosynthesis varies, the pool of less abundant proteins involved in the Calvin cycle (including
101 Rubisco activase or enzymes with a high control coefficient in the cycle) or light reactions could
102 change within a few hours. In fact, ¹⁵N labelling has recently shown that some proteins involved
103 in photosynthesis have a short half-life, such as Rubisco activase (turnover rate $\approx 0.2 \text{ d}^{-1}$) [34].

104 Here, we took advantage of omics analyses performed on Arabidopsis rosettes, using
105 gas-exchange under controlled conditions (CO₂, O₂, light/dark) and sampling by instant liquid
106 nitrogen spraying using our system previously described in [35]. Here, it was further combined
107 to isotopic techniques and polysome quantitation to elucidate the potential effect of short-term
108 changes in CO₂ and O₂ mole fraction on protein synthesis. The use of ¹³CO₂ labelling allowed
109 us to quantify the amount of carbon allocated to protein synthesis, while polysome relative
110 quantitation as well as eIFs and RPs phosphorylation analysis (in particular RPS6
111 phosphorylation) gave information on translation activity. The objective of the present study is
112 not to dissect molecular mechanism of translational control but rather, to look at potential
113 changes in protein synthesis with photosynthesis. In fact, our results demonstrate that protein
114 synthesis follows the photosynthesis rate and is unrelated to total amino acid availability,
115 suggesting a control of translation initiation by metabolic signaling driven by the carboxylation-
116 oxygenation balance.

117

118

119 2. Material and methods

120

121 2.1. Plant material

122 After sowing on potting mix, *Arabidopsis thaliana* (Col-0 accession) plantlets were
123 transplanted to individual pots and grown for 6 weeks in a controlled environment (growth
124 chamber) under short days. Conditions were as follows: 8:16 h light/dark at an irradiance of
125 approximately 100 $\mu\text{mol photons m}^{-2} \text{ s}^{-1}$, 20/18°C day/night temperature, 65% humidity and
126 nutrient solution (1 g L⁻¹ PP14-12-32, [Plant-Prod, Puteaux, France] supplemented with 20 μL
127 L⁻¹ fertoligo L [Fertil, Boulogne-Billancourt, France]) twice a week.

128

129 2.2. Metabolomics

130 Metabolomics profiling was performed as in [36]. Briefly, 20 mg of leaf powder from
131 lyophilized leaf samples were extracted with 2 mL methanol:water (70:30 v/v). The supernatant
132 was vacuum dried and chemically derivatized with methoxyamine and MSTFA in pyridine.
133 Ribitol was added as an internal standard, as well as an alkane mix to calibrate retention index.
134 GC-MS metabolomics analyses were carried out using a Pegasus III GC-TOF-MS system
135 (Leco, France). Peak integration was verified manually for all metabolites to avoid erroneous
136 determinations by the Pegasus software.

137

138 2.3. Gas exchange and sampling

139 *Arabidopsis* plants were taken at fixed time of day in the controlled growth chamber (after about
140 4 h light) and used for gas-exchange and labelling. Gas exchange and sampling were carried
141 out as in [37]. Briefly, photosynthesis and respiration rates were monitored with the gas
142 exchange open system LI-COR 6400/XT (LI-COR, Austin, USA), under a controlled humidity
143 of 80% fixed with a dew-point generator (LI-COR 610). Net photosynthesis (A) was measured
144 in typical conditions (desired CO₂ mole fraction, 21% O₂, 22°C, 280 $\mu\text{mol m}^{-2} \text{ s}^{-1}$ PAR
145 [photosynthetically active radiation], 10% blue). CO₂ mole fraction was either 100, 380 or 1000
146 $\mu\text{mol mol}^{-1}$. O₂ mole fraction was either 0% (pure N₂ used as inlet gas), 21% (ordinary air) or
147 100% (pure O₂). CO₂-free conditions (no CO₂ in inlet gas) were not used here since no ¹³C
148 labelling would have been possible. Gas-exchange was carried out with a purpose-built
149 chamber adapted to three *Arabidopsis* rosettes connected to the sample channel of the LI-COR
150 6400 xt. Air temperature in the chamber was maintained with a water-bath. Leaf rosettes were
151 separated from the below-ground part and soil of the pot by a Plexiglas wall (with specific holes
152 for collars sealed with Terostat®) so as to avoid alteration of gas-exchange by soil and root
153 respiration. The upper wall of the leaf chamber was made of a tight polyvinyl chloride film
154 allowing very fast quenching by liquid N₂ freezing. Further details on the chamber can be found
155 in our previous studies [11, 35, 37]. Photosynthesis was allowed to stabilise under the desired
156 CO₂ and O₂ mole fraction (at 280 $\mu\text{mol photon m}^{-2} \text{ s}^{-1}$ PAR) and after 3 hours, rosettes were
157 instantly frozen and stored at -80°C for further analyses. Rosettes sampled in darkness were
158 collected after 3 hours at 380 $\mu\text{mol mol}^{-1}$ CO₂ and 21% O₂ in the light and then 2 hours of dark-
159 adaptation. Isotopic labelling was carried out with ¹³CO₂ (99% ¹³C, Sigma Aldrich) for 4 hours
160 in the O₂/CO₂ conditions of interest, and sampling was carried out as above at the end of the 4-
161 h labelling time by liquid N₂ freezing.

162

163 2.4. *Phosphoproteomics*

164 The protocol used to carry out quantitative phosphoproteomics analyses was similar to that
165 previously described in [35]. Total (non-phosphorylated) protein analysis was also performed
166 on the same samples to quantify total protein abundance (and therefore check that changes in
167 phosphorylation level are not simply due to changes in total protein content). Protein extraction
168 was carried out using the trichloroacetate/acetone method and protein digestion was performed
169 at an enzyme-to-substrate ratio of 1:50 (w:w) overnight at 37°C with sequencing-grade trypsin
170 (Promega). Stable isotope dimethyl labelling was done according to the on-column protocol of
171 [38] using three different isotopologues of formaldehyde (CH₂O, C²H₂O and ¹³C²H₂O) thereby
172 allowing simultaneous injection of three extracts (each triplet is referred to as ‘triplex’). A
173 sample made of the mixture of all of the samples was dimethylated (with unlabeled methyl
174 groups) and used as a reference in all triplexes. The use of triplexes thus allowed us to analyze
175 two samples per injection (intermediate and heavy labeling). After being spin-dried and
176 resuspended in acetonitrile/formic acid solution, peptides were subjected to SCX (Strong
177 Cation Exchange) chromatography. Collected fractions were enriched in phosphopeptides by
178 IMAC (Immobilized ion Metal Affinity Chromatography) [39] and then analysed by nanoLC-
179 MS/MS using a NanoLC-Ultra system (Eksigent). Peptides eluted from a 35-min long, 5-to-
180 35% acetonitrile gradient were analysed with a coupled Q-Exactive mass spectrometer (Thermo
181 Electron). A “Top 8” cycle of data-dependent acquisition was used (i.e., the 8 major ions
182 detected in each MS spectrum were submitted to MS/MS fragmentation). Resolution for
183 precursors and fragments was set to 70,000 and 17,500 respectively. Collision energy was set
184 at 27% and exclusion time at 40 s.

185 For identification of peptides, phosphorylation sites and quantification, database
186 searches were performed using X!Tandem Sledgehammer (2013.09.01.1) [40] with the TAIR
187 database (www.arabidopsis.org). Cysteine carboxyamidomethylation and light, intermediate
188 and heavy dimethylation of peptide N-termini and lysine residues were set as static
189 modifications while methionine oxidation and phosphorylation of tyrosine, serine or threonine
190 residues were set as variable modifications. Mass error tolerance was 10 ppm for precursors
191 and -0.02 Th for fragments. Identified proteins were filtered and grouped using the X!Tandem
192 pipeline v3.3.1 (<http://pappso.inra.fr/bioinfo/xtandempipeline/>) [41]. Relative quantification of
193 non-phosphorylated peptides and phosphopeptides was performed using the MassChroQ
194 software [42] by extracting ion chromatograms (XICs) of all identified peptides within a 5 ppm
195 window and by integrating the area of the XIC peak at their corresponding retention time, after
196 LC-MS/MS chromatogram alignment.

197

198 2.5. *Isotopic measurements in proteins*

199 Proteins were purified from frozen samples (50 mg fresh weight). First, a raw proteic extract
200 was obtained using a trichloroacetate-acetone extraction as above. Then proteins were purified
201 after [43] with the following modifications: the dry pellet (proteins and cell wall debris obtained
202 in the trichloroacetate-acetone extraction) was dissolved in 1.5 mL resuspension buffer (1%
203 SDS, 150 mM Tris-HCl, 0.1 mM dithiothreitol, 1 mM EDTA). After centrifugation at 10,000 g
204 for 5 min at 14°C, the supernatant was collected and proteins were precipitated by adding 1.5
205 mL methanol. After centrifugation (10,000 g, 5 min, 14°C), the supernatant was discarded and
206 the protein pellet rinsed with 1.5 mL methanol and centrifuged. The pellet was then freeze-

207 dried, weighed in tin capsules and analysed. Isotopic analysis was done using an elemental
208 analyser (Carlo-Erba) coupled to an isotope ratio mass spectrometer (Isoprime, Elementar) run
209 in continuous flow. All sample batches included standards (sucrose, glycine, cysteine;
210 previously calibrated against IAEA standards glutamic acid USGS-40 and caffeine IAEA-600)
211 each twelve samples. The isotope composition ($\delta^{13}\text{C}$) was then converted to $\%^{13}\text{C}$.

212

213 2.6. *Polysome abundance*

214 Polysome abundance was determined by sucrose density gradient centrifugation analysis from
215 liquid-nitrogen frozen rosettes (protocol explained in Supplemental Methods).

216

217 2.7. *Statistics*

218 Phosphoproteomics and metabolomics analyses were carried out 3 to 6 times for each condition.
219 Peptides considered to vary significantly between photosynthetic (CO_2/O_2 and/or light/dark)
220 conditions were those with $P < 0.05$ using ANOVA (Fig. 4). This value ensured an acceptable
221 false discovery rate (FDR), estimated as in Tan & Xu (2014), including the Hochberg-
222 Benjamini correction (Hochberg & Benjamini 1990), over the whole dataset. A multivariate
223 analysis was carried out with orthogonal projection on latent structures (OPLS, with
224 phosphopeptides or metabolites as X variables and O_2/CO_2 conditions as a quantitative Y
225 variable) carried out with Simca (MKS Umetrics, Sweden) [44, 45]. The effect of each
226 phosphopeptide or metabolite in explaining the X-Y relationship was quantified using the
227 loading along axis 1 ($p_{\text{corr}}(1)$) and the P -value of the ANOVA in a volcano plot. The robustness
228 of the OPLS model was assessed with the correlation coefficient between prediction and
229 observations (R^2), the cross-validated correlation coefficient (Q^2) and the intercept of the
230 response of Q^2 to similarity in iterated (250 iterations) permutations tests (Q^2_{int}). The statistical
231 significance of the OPLS model was tested using a χ^2 test on the comparison with a random
232 model (mean \pm random error). The associated P -value was denoted as $P_{\text{CV-ANOVA}}$.

233

234

235 3. Results

236

237 3.1. Photosynthesis and metabolism

238 Six gas-exchange conditions were used, with CO₂ mole fraction of 100, 380 or 1000 μmol mol⁻¹
239 ¹ under 21% O₂, and O₂ mole fraction of 0% (pure N₂ used as background gas), 21% or 100%
240 (pure O₂ as background gas) at 380 μmol mol⁻¹ CO₂. Analyses were also conducted in dark-
241 adapted rosettes after photosynthesis under standard (21% O₂, 380 μmol mol⁻¹ CO₂) conditions.
242 Changes in photosynthetic conditions were associated with considerable changes in metabolite
243 content. Metabolomics analyses by GC-MS showed that amongst the 108 analytes detected, 31
244 were associated with significant changes ($P < 0.01$ with an ANOVA) with O₂/CO₂ conditions
245 (Fig. 1a). They could be grouped into three clusters. The first cluster comprised alanine and
246 tyrosine, considerably increased with N₂ (0% O₂) as inlet air (meaning ≈0.02% O₂ in air
247 surrounding leaves due to photosynthetic O₂ evolution). The second cluster comprised
248 metabolites particularly accumulated at very high photorespiration (low photosynthesis), such
249 as glycine and serine (photorespiration intermediates) but also other amino acids such as
250 cysteine, threonine and valine, or organic acids such as succinate. The third cluster comprised
251 metabolites present under normoxic conditions and decreased under 0% O₂ inlet air, such as
252 glycolate (photorespiration intermediate), fumarate or putrescine. Unsurprisingly, several
253 metabolites (including sugars and photorespiratory intermediates glycine and serine) were
254 affected by darkness as compared to the light (Fig. S2). Multivariate analysis yielded a very
255 good OPLS model ($R^2 = 0.965$; $Q^2 = 0.934$) that was robust (negative Q^2_{int} at -0.501) and highly
256 significant ($P_{\text{CV-ANOVA}} = 4 \cdot 10^{-14}$) (Fig. S1). The volcano plot that combines univariate and
257 multivariate analysis showed that best biomarkers of O₂/CO₂ conditions were succinate, serine,
258 glycine, pipecolate and cysteine (decreased with photosynthesis), and alanine and homoserine
259 (increased at high photosynthesis) (Fig. 1b).

260 As expected, there was a clear increase in the photosynthesis rate as O₂/CO₂ decreased
261 (showing the inhibition of photorespiration and augmented carboxylation as the O₂-to-CO₂ ratio
262 decreased), with a significant depressing effect of low O₂ (Fig. 1c). There was no significant
263 effect of O₂ mole fraction on the rate of dark respiration (CO₂ evolution in darkness). The sum
264 of proteogenic amino acids (expressed in signal % of total recovered metabolites) tended to
265 increase as CO₂ increased from 100 to 1000 μmol mol⁻¹, but there was also a high content in
266 amino acids at very high photorespiration (100% O₂) and in darkness (Fig. 1d). These effects
267 were driven by the accumulation of alanine at low O₂, the build-up of glycine and serine at
268 100% O₂, and the proportional lower content in sugars in darkness. The impact of
269 photorespiration on glycine and serine metabolism was also visible with the glycine-to-serine
270 ratio that increased considerably under 100% O₂ (Fig. 1e).

271

272 3.2. Carbon allocation to protein synthesis

273 Isotopic labelling with ¹³CO₂ during photosynthesis was carried out in order to follow the
274 metabolic partitioning of fixed carbon into proteins. Labelling with ¹³CO₂ was obviously not
275 performed in the dark since there was no photosynthetic CO₂ fixation. There was a clear ¹³C
276 incorporation into proteins as shown by the ¹³C percentage above natural abundance (Fig. 2a).
277 When converted into absolute units (accounting for both leaf protein content and % ¹³C), the
278 allocation flux to proteins increased up to four times as the O₂/CO₂ ratio decreased showing the

279 impact of source carbon fixation to protein synthesis (Fig. 2b). In fact, at low oxygen, the ¹³C
280 flux represented about 0.2 μmol m⁻² s⁻¹. However, when normalized to photosynthesis,
281 allocation fell within a narrow range of 1 to 2.5% of photosynthesis, with higher values at 100%
282 O₂ perhaps suggesting a specific effect of high oxygen on protein synthesis.

283

284 3.3. Polysome abundance

285 Polysome abundance was measured using the gradient method based on absorbance at 260 nm
286 using the signal of the polysome gradient region (Fig. 3a). There was a substantial difference
287 in particular when comparing low O₂/CO₂ to other conditions: in fact, when expressed in
288 normalized units (% of total trace signal), polysome relative abundance was significantly higher
289 at high photosynthesis (Fig. 3b). Polysome abundance tended to be lower at high
290 photorespiration (100% O₂) compared to that in darkness. Also, as expected, there was a
291 significant effect of O₂ mole fraction in darkness with less polysomes at low oxygen,
292 highlighting the specific effect of hypoxia. Of course, this analysis encompasses all polysome
293 fractions in the same peak (organellar and cytosolic) but taken as a whole, the polysome content
294 was found to be affected by gaseous conditions, and in the light, correlated to the photosynthetic
295 rate.

296

297 3.4. Phosphorylation of eIFs and RPs

298 The phosphoproteomics analysis allowed the detection and quantification of 2,057
299 phosphopeptides (representing 1,044 individual proteins), among which 69 (3.3%) were
300 associated with protein synthesis (translation elongation factors, translation initiation factors,
301 ribosomal proteins and other proteins associated with translation). The list of unique
302 phosphopeptides is provided in Table 1 and some of them are illustrated in Fig. 4. Phosphosites
303 identified here have been found previously, except for two of them: Ser 47/Thr 51 in the
304 nucleus-encoded chloroplastic ribosomal protein RPS9 (AT1G74970), and Ser 149 of eIF2Bδ
305 (AT1G48970) (Table 1). Phosphopeptides were filtered to carry out statistics, by keeping only
306 those with less than 20% missing values. Univariate analysis with ANOVA conducted with the
307 69 translation-related phosphopeptides, showed that 17 phosphopeptides were significantly
308 affected by O₂/CO₂ conditions, representing 11 proteins (Fig. 4a). Hierarchical clustering
309 showed that there were distributed in two groups. The first cluster was associated with higher
310 phosphorylation at high photosynthesis and comprised RPS6A and RPS6B at phosphosite Ser
311 240 (detailed in Fig. 4b). The second cluster was associated with lower phosphorylation as
312 photosynthesis increased (and higher phosphorylation in the dark) and comprised eIF4G at
313 phosphosites Ser 178 (detailed in Fig. 4b). Multivariate analysis conducted on the 69
314 translation-related phosphopeptides yielded a very good OPLS model (R² = 0.954; Q² = 0.916)
315 that was robust (negative Q²_{int} at -0.265) and highly significant (P_{CV-ANOVA} = 7·10⁻¹³) (Fig. 4c).
316 The volcano plot that combines univariate and multivariate analysis showed that best
317 biomarkers of O₂/CO₂ conditions were RPS6 and eIF3d phosphopeptides (increased with
318 photosynthesis), and eIF4G and eIF5A2 phosphopeptides (decreased at high photosynthesis)
319 (Fig. 4d). Taken as a whole, the phosphopattern found here indicates that phosphorylation that
320 promoted translation (such as RPS6 phosphorylation) increased while phosphorylation that
321 inhibits translation (such as eIF4G) decreased with photosynthesis. Changes observed here in
322 phosphopeptide abundance were not due to changes in total protein amounts but were

323 effectively due to modifications in phosphorylation level, since none of the significant
324 phosphopeptides were associated with significant variation in total protein content (Fig. S3).
325
326

327 4. Discussion

328

329 4.1. Protein synthesis increases with CO₂/O₂

330 We find that the ¹³C-flux to proteins increases with photosynthesis (Fig. 2b) and our estimate
331 of the absolute carbon allocation to protein synthesis was 0.1-0.2 μmol m⁻² s⁻¹, that is, 3 to 6 μg
332 protein m⁻² s⁻¹. This estimate agrees with the order of magnitude of protein turnover rate
333 estimated using inhibitors (≈0.2 μmol C m⁻² s⁻¹) [46] or ¹⁴C-tracing (between 0.1 and 0.25 μmol
334 m⁻² s⁻¹ depending on light conditions) [33] and the average protein synthesis rate of 6.25 μg
335 protein m⁻² s⁻¹ (assuming a specific leaf area of 180 g FW m⁻²) found in Arabidopsis rosettes
336 using ¹³C labelling [6].

337 **The physiological impact of protein synthesis not only relates to carbon allocation but**
338 **also to energy consumption since translation consumes a substantial amount of ATP.** In effect,
339 the average amount of ATP required per amino acid added during translation is about 5 [47].
340 **The order of magnitude of the rate associated with protein synthesis (0.1-0.2 μmol C m⁻² s⁻¹)**
341 **represents** an ATP budget of ≈0.25 μmol ATP m⁻² s⁻¹. Of course, the rate of protein synthesis
342 was obtained via isotope labelling and includes not only cytoplasmic but also chloroplastic
343 protein synthesis. **Therefore, the ATP demand must be met by both photosynthetic light**
344 **reactions in the chloroplast and** day respiration in the cytoplasm.

345 **It is worth noting that** day respiration generates about 0.5 μmol CO₂ m⁻² s⁻¹ [48] i.e. 2.6
346 μmol ATP m⁻² s⁻¹ (using a conversion factor of 31.5 ATP per catabolized glucose molecule)
347 and thus, protein synthesis represents about 0.25/2.6 = 10% of metabolic energy generated by
348 day respiration. **That said, cytoplasmic ATP not only comes from catabolism (reoxidation of**
349 **NADH produced by day respiratory metabolism) but also from photorespiration (reoxidation**
350 **of photorespiratory NADH coming from glycine-to-serine conversion), which in turn depends**
351 **on CO₂ and O₂. The contribution of photorespiration to meet the ATP demand might** explain
352 why protein synthesis was found here to decline more slowly than photosynthesis when the
353 O₂/CO₂ ratio increased (i.e., 2% of photosynthesis at high O₂ vs. 1% of photosynthesis at high
354 CO₂; Fig. 2c) despite the down-regulation of translation (**further explained below**). This would
355 be consistent with the non-quantitative recycling of photorespiratory intermediates such as
356 glycerate at high photorespiration [49]. In other words, ATP that is not used to reform 3-
357 phosphoglycerate from glycerate could have been used by other processes such as protein
358 synthesis.

359 The increase in ¹³C-allocation when CO₂/O₂ increased was accompanied by an increased
360 proportion of ribosomes in polysomes (Fig. 3) demonstrating an augmented translational
361 activity. Furthermore, this correlated with a significant increase in RPS6 phosphorylation at Ser
362 240 (substrate phosphosite of RPS6 kinase) (Fig. 4) which is **usually** typical of the stimulation
363 of ribosomal activity to initiate translation (**but see [50] in yeast**). There was also a stimulation
364 of translation initiation via the phosphorylation of a number of eIFs, such as eIF4B2 (further
365 discussed below). Taken as a whole, our data show that when the CO₂-to-O₂ ratio increases,
366 there is an increase in protein synthesis (in absolute terms, i.e. in moles of ¹³C committed to
367 protein production) and this is reflected by higher translational activity.

368

369 4.2. Involvement of protein phosphorylation

370 In addition to RPS6, we found that other proteins involved in translation were phosphorylated,
371 with significant changes with O₂/CO₂ (Fig. 4). Unfortunately, the role of phosphorylation is not
372 always well-known for many initiation factors eIFs (or ribosomal proteins). Phosphorylation
373 might be linked to mechanisms of regulation of translation under our conditions. For example,
374 it seems that eIF4G phosphorylation (at Ser 178) inhibits translation as photorespiration
375 increases while eIF4B2 and eIF3d phosphorylation stimulates translation as photosynthesis
376 increases (for further details on potential roles of phosphorylation sites, see Supplementary
377 Text). In addition to eIFs, our analysis found that phosphorylation of the elongation factor
378 eEF5A2 (also known as initiation factor eIF5A) anti-correlated with photosynthesis, suggesting
379 that translation down-regulation also involves an inhibition of elongation. While eEF5
380 phosphorylation (at Ser 2) is poorly documented in plants and has been suggested to have no
381 effect in yeast, eEF5 activity is also known to be controlled by hypusination at the consensus
382 site K-x-G-(^{Hyp}K)-H-G-x-A-K **in yeast and Mammals** (for a review, see [51]). A hypusination
383 site is present in Arabidopsis eEF5 (at Lys 51) and hypusination has been shown to occur in
384 planta [52]. Here, hypusination could not be analyzed (in fact, the hypusination site GKHG is
385 cleaved by trypsin). There was no correlation between translation activity (photosynthesis) and
386 the content in hypusine precursors, polyamines (Fig. S4).

387 Amongst phosphopeptides with more than 20% missing data, one possessed a clear
388 trend with photosynthesis (missing data mostly corresponded to samples collected in the dark)
389 and was associated with nucleolin (NUC-L1; Table 1). There was a clear positive relationship
390 between photosynthesis and nucleolin phosphorylation (Fig. S5). Nucleolin has been shown to
391 be associated with a variety of cellular processes including in plants [53, 54]. Nucleolin
392 phosphorylation has been extensively documented in Mammals, where CK2-mediated
393 phosphorylation triggers nucleolin relocation to the cytoplasm and stimulates its helicase
394 activity so as to facilitate internal ribosomal entry and translation of specific mRNAs [55-57].
395 In fact, the phosphosite found here at Ser 163 corresponds to a typical CK2 phosphorylation
396 motif (with at least two acidic residues downstream of phosphorylated Ser) (Table 1).

397 It is worth noting that RPS6A and B were not the sole RPs detected here, since we also
398 found phosphopeptides associated with RPP1A/2A, significantly less abundant at high
399 photosynthesis (high CO₂, low O₂) (Fig. 4). It suggests that unlike RPS6, phosphorylation of
400 these two RPs inhibits translation. This agrees with the recognized role of phosphorylation at
401 the C-terminus (here, Ser 102/120) by CK2 in promoting RPP1/RPP2 dissociation and RPP1
402 degradation in yeast [58-60].

403

404 *4.3. Potential mechanisms*

405 Our data suggest that phosphorylation events play an important role in regulating translation
406 activity when O₂/CO₂ varies, as reflected by the progressive RPS6 phosphorylation. RPS6 is
407 phosphorylated by RPS6 kinase (S6K) which is in turn activated (phosphorylated) via the
408 mTOR pathway. Also recently, **in Arabidopsis**, MRF1 (MA3 domain-containing translation
409 regulatory factor 1) has been shown to interact physically with eIF4A and appears to be
410 phosphorylated via mTOR [61]. eIF2Bδ1 has recently been shown to be a direct
411 phosphorylation target of mTOR **in Arabidopsis** (eIF2Bδ1 being more phosphorylated in the
412 presence of sucrose) at the same phosphosite as that found here [62]. More generally, several
413 eIFs have been shown to be amongst phosphorylation targets of the mTOR pathway, such as

414 eIF4G, eIF4B1, eIF2 β 1 and eIF6A [62]. Since the mTOR pathway mediates nutrient signaling
415 [63], it might suggest that the cellular content in free sugars and/or amino acids drive the
416 response observed here. However, under our conditions, there was no relationship between total
417 amino acid content and protein synthesis (Figs. 1-3). Similarly, there was no correlation
418 between protein synthesis and sucrose content since sucrose (which was rather variable)
419 appeared to be significantly lower under both low and high O₂ (Fig. S4). To gain insight on
420 possible relationships with metabolites, we conducted a correlation analysis between
421 metabolites and phosphosites (Fig. S6). As expected, multivariate analysis showed there was a
422 positive relationship between significant phosphosites (such as RPS6B) and metabolites driven
423 by O₂/CO₂ such as fructose or alanine (and a negative relationship with photorespiratory
424 metabolites glycine and serine) (Fig. S6a). Direct regression analysis also showed a negative
425 relationship between eIF2B α phosphorylation (significantly enhanced at 100% O₂, Fig. 4) and
426 sugars maltose and trehalose (Fig. S6b). It is thus likely that metabolic **signalling participating
427 in phosphorylation changes involved** (i) a metabolite other than sucrose or amino acids (such
428 as triose phosphates or trehalose 6-phosphate) and/or (ii) another pathway interacting with
429 mTOR, such as SnRK1 signaling which is believed to interact with mTOR, and has been shown
430 to inhibit mTOR-mediated RPS6 phosphorylation **in plants** [64, 65]. **The possible involvement
431 of SnRK1 is further discussed in the Supplementary Text.**

432

433 *4.4. Conclusions and perspectives*

434 Taken as a whole, our results show that cytoplasmic protein synthesis increases with
435 photosynthesis via the stimulation of translation initiation. The molecular mechanism of this
436 effect involves protein phosphorylation, in particular of RPs and eIFs. However, other
437 mechanisms not examined here could have contributed, such as changes in mRNA stability or
438 upstream open reading frames (uORF) translation that can mediate metabolic sensing and
439 control ribosome dissociation from specific mRNAs [66, 67]. We recognize that (i) the present
440 analysis was focused on protein synthesis while protein degradation might be affected by
441 photosynthetic conditions and (ii) the stimulation of cytoplasmic translation is likely to concern
442 specific mRNAs leading to differential protein turnover (for example, proteins involved in
443 photosynthesis might be synthesized more actively when photosynthesis increases). Also, it
444 could be interesting to examine molecular mechanisms further, for example by measuring
445 mTOR activity in different photosynthetic contexts. These aspects will be addressed in a
446 subsequent study.

447

448

449 **Acknowledgements**

450 The authors acknowledge the support by public grants overseen by the French National
451 Research Agency (ANR) through a Jeunes Chercheurs project (contract 12-0001-01) and the
452 *Investissement d'Avenir* program through the Labex Saclay Plant Sciences (ANR-10-LABX-
453 0040-SPS) for a post-doctoral grant (to S.M.). G.T and C.A. also thank the Australian Research
454 Council for its support through a *Future Fellowship* grant, under contract FT140100645. The
455 authors thank the facility *Plateforme Métabolisme-Métabolome* for accessing the GC-MS
456 instrument for metabolomics, and Dr. H. Stuart-Williams (Research School of Biology, ANU)
457 for isotopic measurements. The authors thank Dr. K. Hannan (John Curtin School of Medical
458 Research, ANU) for giving access to instruments to carry out polysome profiling.

459
460 **Contributions**

461
462 S.M. did gas exchange experiments and sampling for metabolomics and proteomics, M.D. and
463 M.Z. did phosphoproteomics analyses, C.A. did metabolomics analyses, A.C. did isotopic
464 labelling and polysome profiling, G.T. carried out data integration and wrote the paper, all
465 authors discussed results and amended the manuscript.

466 **References**

- 467
- 468 [1] M. Rouelle, Observations sur les parties vertes des plantes, et sur la matière glutineuse ou
469 végéto-animale, Journal de Médecine Chirurgie et Pharmacie (Paris), 40 (1773) 59-67.
- 470 [2] A.C. Chibnall, G. Wiltshire, A study with isotopic nitrogen of protein metabolism in
471 detached runner-bean leaves, New Phytologist, 53 (1954) 38-43.
- 472 [3] K. Mothes, Die vakuuminfiltration im ernährungsversuch. (Dargestellt an untersuchungen
473 über die assimilation des ammoniaks), Planta, 19 (1933) 117-138.
- 474 [4] H.B. Vickery, G.W. Pucher, R. Schoenheimer, D. Rittenberg, The assimilation of ammonia
475 nitrogen by the tobacco plant: a preliminary study with isotopic nitrogen, Journal of Biological
476 Chemistry, 135 (1940) 531-539.
- 477 [5] M. Havé, A. Marmagne, F. Chardon, C. Masclaux-Daubresse, Nitrogen remobilization
478 during leaf senescence: lessons from *Arabidopsis* to crops, Journal of Experimental Botany, 68
479 (2016) 2513-2529.
- 480 [6] H. Ishihara, T. Obata, R. Sulpice, A.R. Fernie, M. Stitt, Quantifying protein synthesis and
481 degradation in *Arabidopsis* by dynamic ¹³CO₂ labeling and analysis of enrichment in individual
482 amino acids in their free pools and in protein, Plant Physiology, 168 (2015) 74-93.
- 483 [7] S.K. Pal, M. Liput, M. Piques, H. Ishihara, T. Obata, M.C. Martins, R. Sulpice, J.T. van
484 Dongen, A.R. Fernie, U.P. Yadav, Diurnal changes of polysome loading track sucrose content
485 in the rosette of wild-type *Arabidopsis* and the starchless *pgm* mutant, Plant Physiology, 162
486 (2013) 1246-1265.
- 487 [8] M. Piques, W.X. Schulze, M. Höhne, B. Usadel, Y. Gibon, J. Rohwer, M. Stitt, Ribosome
488 and transcript copy numbers, polysome occupancy and enzyme dynamics in *Arabidopsis*,
489 Molecular Systems Biology, 5 (2009) 314-324.
- 490 [9] D.D. Seaton, A. Graf, K. Baerenfaller, M. Stitt, A.J. Millar, W. Gruissem, Photoperiodic
491 control of the *Arabidopsis* proteome reveals a translational coincidence mechanism, Molecular
492 Systems Biology, 14 (2018) Article e7962.
- 493 [10] H. Ishihara, T.A. Moraes, E.-T. Pyl, W.X. Schulze, T. Obata, A. Scheffell, A.R. Fernie, R.
494 Sulpice, M. Stitt, Growth rate correlates negatively with protein turnover in *Arabidopsis*
495 accessions, The Plant Journal, 91 (2017) 416-429.
- 496 [11] E. Boex-Fontvieille, M. Davenport, M. Jossier, M. Zivy, M. Hodges, G. Tcherkez,
497 Photosynthetic control of *Arabidopsis* leaf cytoplasmic translation initiation by protein
498 phosphorylation, PloS one, 8 (2013) Article e70692.
- 499 [12] K.S. Browning, J. Bailey-Serres, Mechanism of cytoplasmic mRNA translation, in: The
500 *Arabidopsis* book, American Society of Plant Biologists, 2015, pp. Article e0176.
- 501 [13] M.V. Turkina, H.K. Årstrand, A.V. Vener, Differential phosphorylation of ribosomal
502 proteins in *Arabidopsis thaliana* plants during day and night, PloS one, 6 (2011) Article e29307.
- 503 [14] R. Enganti, S.K. Cho, J.D. Toperzer, R.A. Urquidi-Camacho, O.S. Cakir, A.P. Ray, P.E.
504 Abraham, R.L. Hettich, A.G. von Arnim, Phosphorylation of ribosomal protein RPS6 integrates
505 light signals and circadian clock signals, Frontiers in Plant Science, 8 (2018) 2210.
- 506 [15] T. Andreyeva, E. Plyshevskaya, A study with N-15 of protein formation in the
507 photosynthetic process, Proceedings of the Academy of Sciences of USSR, Biology Series
508 (Izvestiia Akademii Nauk SSSR. Seria Biologicheskaja), 87 (1952) 301-310.
- 509 [16] K.S. Browning, Plant translational machinery, in: S. Howel (Ed.) Molecular biology: the
510 plant sciences, Springer New York, 2014, pp. 129-151.
- 511 [17] C. Merchante, A.N. Stepanova, J.M. Alonso, Translation regulation in plants: an
512 interesting past, an exciting present and a promising future, The Plant Journal, 90 (2017) 628-
513 653.

- 514 [18] S. Lageix, S. Rothenburg, T.E. Dever, A.G. Hinnebusch, Enhanced interaction between
515 pseudokinase and kinase domains in GCN2 stimulates eIF2 α phosphorylation in starved cells,
516 PLoS genetics, 10 (2014) Article e1004326.
- 517 [19] T. Dobrenel, E. Mancera-Martínez, C. Forzani, M. Azzopardi, M. Davanture, M. Moreau,
518 M. Schepetilnikov, J. Chicher, O. Langella, M. Zivy, C. Robaglia, L.A. Ryabova, J. Hanson,
519 C. Meyer, The *Arabidopsis* TOR kinase specifically regulates the expression of nuclear genes
520 coding for plastidic ribosomal proteins and the phosphorylation of the cytosolic ribosomal
521 protein S6, *Frontiers in Plant Science*, 7 (2016) Article 1611.
- 522 [20] A.N. Bruns, S. Li, G. Mohannath, D.M. Bisaro, Phosphorylation of *Arabidopsis* eIF4E and
523 eIFiso4E by SnRK1 inhibits translation, *The FEBS Journal*, (2019) In press.
- 524 [21] S. Lageix, E. Lanet, M.-N. Pouch-Pélissier, M.-C. Espagnol, C. Robaglia, J.-M. Deragon,
525 T. Pélissier, *Arabidopsis* eIF2 α kinase GCN2 is essential for growth in stress conditions and is
526 activated by wounding, *BMC plant biology*, 8 (2008) 134-144.
- 527 [22] L. Wang, H. Li, C. Zhao, S. Li, L. Kong, W. Wu, W. Kong, Y. Liu, Y. Wei, J.-K. Zhu, H.
528 Zhang, The inhibition of protein translation mediated by AtGCN1 is essential for cold tolerance
529 in *Arabidopsis thaliana*, *Plant, Cell & Environment*, 40 (2017) 56-68.
- 530 [23] Y. Zhang, Y. Wang, K. Kanyuka, M.A.J. Parry, S.J. Powers, N.G. Halford, GCN2-
531 dependent phosphorylation of eukaryotic translation initiation factor-2 α in *Arabidopsis*, *Journal*
532 *of Experimental Botany*, 59 (2008) 3131-3141.
- 533 [24] M.D. Dennis, K.S. Browning, Differential phosphorylation of plant translation initiation
534 factors by *Arabidopsis thaliana* CK2 holoenzymes, *Journal of Biological Chemistry*, 284
535 (2009) 20602-20614.
- 536 [25] M.D. Dennis, M.D. Person, K.S. Browning, Phosphorylation of plant translation initiation
537 factors by CK2 enhances the in vitro interaction of multifactor complex components, *Journal*
538 *of Biological Chemistry*, 284 (2009) 20615-20628.
- 539 [26] H.-Y. Cho, M.-Y.J. Lu, M.-C. Shih, The SnRK1-eIFiso4G1 signaling relay regulates the
540 translation of specific mRNAs in *Arabidopsis* under submergence, *New Phytologist*, 222 (2019)
541 366-381.
- 542 [27] J. Walkley, Protein synthesis in mature and senescent leaves of barley, *New Phytologist*,
543 39 (1940) 362-369.
- 544 [28] R. Dickson, P. Larson, Incorporation of ¹⁴C-photosynthate into major chemical fractions
545 of source and sink leaves of cottonwood, *Plant Physiology*, 56 (1975) 185-193.
- 546 [29] R.E. Dickson, P.R. Larson, ¹⁴C fixation, metabolic labeling patterns, and translocation
547 profiles during leaf development in *Populus deltoides*, *Planta*, 152 (1981) 461-470.
- 548 [30] J. Hellebust, R. Bidwell, Protein turnover in wheat and snapdragon leaves: preliminary
549 investigations, *Canadian Journal of Botany*, 41 (1963) 969-983.
- 550 [31] G. Tcherkez, A.M. Limami, Net photosynthetic CO₂ assimilation: more than just CO₂ and
551 O₂ reduction cycles, *New Phytologist*, (2019) In press.
- 552 [32] N.J. Roberts, R.C. Menary, Partitioning and distribution of ¹⁴C in *Boronia megastigma*
553 Nees, *Journal of Plant Physiology*, 137 (1990) 135-139.
- 554 [33] A.J. Escobar-Gutiérrez, J.-P. Gaudillère, Carbon partitioning in source leaves of peach, a
555 sorbitol-synthesizing species, is modified by photosynthetic rate, *Physiologia Plantarum*, 100
556 (1997) 353-360.
- 557 [34] L. Li, C.J. Nelson, J. Trösch, I. Castleden, S. Huang, A.H. Millar, Protein degradation rate
558 in *Arabidopsis thaliana* leaf growth and development, *The Plant Cell*, 29 (2017) 207-228.
- 559 [35] C. Abadie, S. Mainguet, M. Davanture, M. Hodges, M. Zivy, G. Tcherkez, Concerted
560 changes in the phosphoproteome and metabolome under different CO₂/O₂ gaseous conditions
561 in *Arabidopsis* rosettes, *Plant and Cell Physiology*, 57 (2016) 1544-1556.

562 [36] C. Bathellier, G. Tcherkez, C. Mauve, R. Bligny, E. Gout, J. Ghashghaie, On the resilience
563 of nitrogen assimilation by intact roots under starvation, as revealed by isotopic and
564 metabolomic techniques, *Rapid Communications in Mass Spectrometry*, 23 (2009) 2847-2856.
565 [37] E. Boex-Fontvieille, M. Davanture, M. Jossier, M. Zivy, M. Hodges, G. Tcherkez,
566 Photosynthetic activity influences cellulose biosynthesis and phosphorylation of proteins
567 involved therein in *Arabidopsis* leaves, *Journal of experimental botany*, 65 (2014) 4997-5010.
568 [38] P.J. Boersema, R. Raijmakers, S. Lemeer, S. Mohammed, A.J. Heck, Multiplex peptide
569 stable isotope dimethyl labeling for quantitative proteomics, *Nature Protocols*, 4 (2009) 484-
570 494.
571 [39] X. Yue, A. Schunter, A.B. Hummon, Comparing multistep immobilized metal affinity
572 chromatography and multistep TiO₂ methods for phosphopeptide enrichment, *Analytical*
573 *Chemistry*, 87 (2015) 8837-8844.
574 [40] R. Craig, R.C. Beavis, TANDEM: matching proteins with tandem mass spectra,
575 *Bioinformatics*, 20 (2004) 1466-1467.
576 [41] O. Langella, B. Valot, T. Balliau, M.I. Blein-Nicolas, L. Bonhomme, M. Zivy,
577 X!TandemPipeline: a tool to manage sequence redundancy for protein inference and
578 phosphosite identification, *Journal of Proteome Research*, 16 (2016) 494-503.
579 [42] B. Valot, O. Langella, E. Nano, M. Zivy, MassChroQ: a versatile tool for mass
580 spectrometry quantification, *Proteomics*, 11 (2011) 3572-3577.
581 [43] T. Isaacson, C.M. Damasceno, R.S. Saravanan, Y. He, C. Catalá, M. Saladié, J.K. Rose,
582 Sample extraction techniques for enhanced proteomic analysis of plant tissues, *Nature*
583 *Protocols*, 1 (2006) 769-774.
584 [44] L. Eriksson, J. Trygg, S. Wold, CV-ANOVA for significance testing of PLS and OPLS®
585 models, *Journal of Chemometrics: A Journal of the Chemometrics Society*, 22 (2008) 594-600.
586 [45] M. Bylesjö, M. Rantalainen, O. Cloarec, J.K. Nicholson, E. Holmes, J. Trygg, OPLS
587 discriminant analysis: combining the strengths of PLS-DA and SIMCA classification, *Journal*
588 *of Chemometrics: A Journal of the Chemometrics Society*, 20 (2006) 341-351.
589 [46] T.J. Bouma, R. De Visser, J.H.J.A. Janssen, M.J. De Kock, P.H. Van Leeuwen, H.
590 Lambers, Respiratory energy requirements and rate of protein turnover in vivo determined by
591 the use of an inhibitor of protein synthesis and a probe to assess its effect, *Physiologia*
592 *Plantarum*, 92 (1994) 585-594.
593 [47] F.W.T. Penning De Vries, The cost of maintenance processes in plant cells, *Annals of*
594 *Botany*, 39 (1975) 77-92.
595 [48] G. Tcherkez, P. Gauthier, T.N. Buckley, F.A. Busch, M.M. Barbour, D. Bruhn, M.A.
596 Heskell, X.Y. Gong, K.Y. Crous, K. Griffin, Leaf day respiration: low CO₂ flux but high
597 significance for metabolism and carbon balance, *New Phytologist*, 216 (2017) 986-1001.
598 [49] C. Abadie, C. Bathellier, G. Tcherkez, Carbon allocation to major metabolites in
599 illuminated leaves is not just proportional to photosynthesis when gaseous conditions (CO₂ and
600 O₂) vary, *New Phytologist*, 218 (2018) 94-106.
601 [50] S. Yerlikaya, M. Meusburger, R. Kumari, A. Huber, D. Anrather, M. Costanzo, C. Boone,
602 G. Ammerer, P.V. Baranov, R. Loewith, TORC1 and TORC2 work together to regulate
603 ribosomal protein S6 phosphorylation in *Saccharomyces cerevisiae*, *Molecular Biology of the*
604 *Cell*, 27 (2016) 397-409.
605 [51] T.E. Dever, E. Gutierrez, B.-S. Shin, The hypusine-containing translation factor eIF5A,
606 *Critical Reviews in Biochemistry and Molecular Biology*, 49 (2014) 413-425.
607 [52] B. Belda-Palazón, C. Almendáriz, E. Martí, J. Carbonell, A. Ferrando, Relevance of the
608 axis spermidine/eIF5A for plant growth and development, *Frontiers in Plant Science*, 7 (2016)
609 Article 245.
610 [53] F. Pontvianne, I. Matía, J. Douet, S. Tourmente, F.J. Medina, M. Echeverria, J. Sáez-
611 Vásquez, Characterization of AtNUC-L1 reveals a central role of nucleolin in nucleolus

612 organization and silencing of AtNUC-L2 gene in *Arabidopsis*, *Molecular Biology of the Cell*,
613 18 (2007) 369-379.

614 [54] M. Tajrishi, R. Tuteja, N. Tuteja, Nucleolin: the most abundant multifunctional
615 phosphoprotein of nucleolus, *Communicative and Integrative Biology*, 4 (2011) 267-275.

616 [55] D.-m. Wu, P. Zhang, R.-y. Liu, Y.-x. Sang, C. Zhou, G.-c. Xu, J.-l. Yang, A.-p. Tong, C.-
617 t. Wang, Phosphorylation and changes in the distribution of nucleolin promote tumor metastasis
618 via the PI3K/Akt pathway in colorectal carcinoma, *FEBS letters*, 588 (2014) 1921-1929.

619 [56] N. Tuteja, N.W. Huang, D. Skopac, R. Tuteja, S. Hrvatic, J. Zhang, S. Pongor, G. Joseph,
620 C. Faucher, F. Amalric, A. Falaschi, Human DNA helicase IV is nucleolin, an RNA helicase
621 modulated by phosphorylation, *Gene*, 160 (1995) 143-148.

622 [57] M. Schwab, C. Dreyer, Protein phosphorylation sites regulate the function of the bipartite
623 NLS of nucleolin, *European journal of cell biology*, 73 (1997) 287-297.

624 [58] M. Tchorzewski, A. Boguszewska, P. Dukowski, N. Grankowski, Oligomerization
625 properties of the acidic ribosomal P-proteins from *Saccharomyces cerevisiae*: effect of P1A
626 protein phosphorylation on the formation of the P1A-P2B hetero-complex, *Biochimica et*
627 *Biophysica Acta (BBA)-Molecular Cell Research*, 1499 (2000) 63-73.

628 [59] P. Hasler, N. Brot, H. Weissbach, A.P. Parnassa, K.B. Elkon, Ribosomal proteins P0, P1,
629 and P2 are phosphorylated by casein kinase II at their conserved carboxyl termini, *Journal of*
630 *Biological Chemistry*, 266 (1991) 13815-13820.

631 [60] G. Nusspaumer, M. Remacha, J.P.G. Ballesta, Phosphorylation and N-terminal region of
632 yeast ribosomal protein P1 mediate its degradation, which is prevented by protein P2, *The*
633 *EMBO Journal*, 19 (2000) 6075-6084.

634 [61] D.-H. Lee, S.J. Park, C.S. Ahn, H.-S. Pai, *MRF* family genes are involved in translation
635 control, especially under energy-deficient conditions, and their expression and functions are
636 modulated by the TOR signaling pathway, *The Plant Cell*, 29 (2017) 2895-2920.

637 [62] J. Van Leene, C. Han, A. Gadeyne, D. Eeckhout, C. Matthijs, B. Cannoot, N. De Winne,
638 G. Persiau, E. Van De Slijke, B. Van de Cotte, Capturing the phosphorylation and protein
639 interaction landscape of the plant TOR kinase, *Nature Plants*, 5 (2019) 316-327.

640 [63] Y. Xiong, J. Sheen, The role of target of rapamycin signaling networks in plant growth and
641 metabolism, *Plant Physiology*, 164 (2014) 499-512.

642 [64] E. Nukarinen, T. Nägele, L. Pedrotti, B. Wurzinger, A. Mair, R. Landgraf, F. Börnke, J.
643 Hanson, M. Teige, E. Baena-Gonzalez, W. Dröge-Laser, W. Weckwerth, Quantitative
644 phosphoproteomics reveals the role of the AMPK plant ortholog SnRK1 as a metabolic master
645 regulator under energy deprivation, *Scientific Reports*, 6 (2016) Article 31697.

646 [65] E. Baena-González, J. Hanson, Shaping plant development through the SnRK1–TOR
647 metabolic regulators, *Current Opinion in Plant Biology*, 35 (2017) 152-157.

648 [66] A. Srivastava, Y. Lu, G. Zinta, Z. Lang, J. Zhu, UTR-dependent control of gene expression
649 in plants, *Trends in Plant Science*, 23 (2018) 248-260.

650 [67] A.G. von Arnim, Q. Jia, J.N. Vaughn, Regulation of plant translation by upstream open
651 reading frames, *Plant Science*, 214 (2014) 1-12.

652 [68] A. Mastroph, M.E. Zanetti, C.J.H. Jang, H.E. Holtan, P.P. Repetti, D.W. Galbraith, T.
653 Girke, J. Bailey-Serres, Profiling translomes of discrete cell populations resolves altered
654 cellular priorities during hypoxia in *Arabidopsis*, *Proceedings of the National Academy of*
655 *Sciences*, 106 (2009) 18843-18848.

656 [69] B. Bai, A. Peviani, S. van der Horst, M. Gamm, B. Snel, L. Bentsink, J. Hanson, Extensive
657 translational regulation during seed germination revealed by polysomal profiling, *New*
658 *Phytologist*, 214 (2017) 233-244.

659 [70] T.C. Vary, C.J. Lynch, Nutrient signaling components controlling protein synthesis in
660 striated muscle, *The Journal of Nutrition*, 137 (2007) 1835-1843.

661 [71] J. Ling, S.J. Morley, J.A. Traugh, Inhibition of cap-dependent translation via
662 phosphorylation of eIF4G by protein kinase Pak2, *The EMBO Journal*, 24 (2005) 4094-4105.
663 [72] S.J. Morley, P.S. Curtis, V.M. Pain, eIF4G: translation's mystery factor begins to yield its
664 secrets, *RNA*, 3 (1997) 1085-1104.
665 [73] A. Marintchev, G. Wagner, Translation initiation: structures, mechanisms and evolution,
666 *Quarterly Reviews of Biophysics*, 37 (2004) 197-284.
667 [74] M. Schepetilnikov, M. Dimitrova, E. Mancera-Martínez, A. Geldreich, M. Keller, L.A.
668 Ryabova, TOR and S6K1 promote translation reinitiation of uORF-containing mRNAs via
669 phosphorylation of eIF3h, *The EMBO journal*, 32 (2013) 1087-1102.
670 [75] H. Ehsan, W.K. Ray, B. Phinney, X. Wang, S.C. Huber, S.D. Clouse, Interaction of
671 *Arabidopsis* BRASSINOSTEROID-INSENSITIVE 1 receptor kinase with a homolog of
672 mammalian TGF- β receptor interacting protein, *The Plant Journal*, 43 (2005) 251-261.
673 [76] A.S.Y. Lee, P.J. Kranzusch, J.A. Doudna, J.H.D. Cate, eIF3d is an mRNA cap-binding
674 protein that is required for specialized translation initiation, *Nature*, 536 (2016) 96-100.
675 [77] P. Crozet, L. Margalha, A. Confraria, A. Rodrigues, C. Martinho, M. Adamo, C.A. Elias,
676 E. Baena-González, Mechanisms of regulation of SNF1/AMPK/SnRK1 protein kinases,
677 *Frontiers in Plant Science*, 5 (2014) Article 190.
678 [78] C.M. Figueroa, J.E. Lunn, A tale of two sugars: trehalose 6-phosphate and sucrose, *Plant*
679 *Physiology*, 172 (2016) 7-27.
680 [79] B. Wurzinger, A. Mair, K. Fischer-Schrader, E. Nukarinen, V. Roustan, W. Weckwerth,
681 M. Teige, Redox state-dependent modulation of plant SnRK1 kinase activity differs from
682 AMPK regulation in animals, *FEBS letters*, 591 (2017) 3625-3636.
683 [80] E. Lewandowska-Gnatowska, L. Szymona, M. Łebska, J. Szczegieliński, G. Muszyńska,
684 Phosphorylation of maize eukaryotic translation initiation factor on Ser2 by catalytic subunit
685 CK2, *Molecular and Cellular Biochemistry*, 356 (2011) 241-251.
686 [81] J.J. Mulekar, E. Huq, Expanding roles of protein kinase CK2 in regulating plant growth
687 and development, *Journal of Experimental Botany*, 65 (2013) 2883-2893.
688 [82] I.C. Vélez-Bermúdez, M. Riera, Maize RNA-Binding Protein ZmTGH: A New Partner for
689 CK2 β 1 Regulatory Subunit, in: K. Ahmed, O.-G. Issinger, R. Szyszka (Eds.) *Protein Kinase*
690 *CK2 Cellular Function in Normal and Disease States*, Springer International Publishing, Cham,
691 2015, pp. 49-55.
692 [83] J. Zhu, W.-S. Wang, D. Ma, L.-Y. Zhang, F. Ren, T.-T. Yuan, A role for CK2 β subunit 4
693 in the regulation of plant growth, cadmium accumulation and H₂O₂ content under cadmium
694 stress in *Arabidopsis thaliana*, *Plant Physiology and Biochemistry*, 109 (2016) 240-247.
695 [84] J. Chen, Y. Wang, F. Wang, J. Yang, M. Gao, C. Li, Y. Liu, Y. Liu, N. Yamaji, J.F. Ma,
696 J. Paz-Ares, L. Nussaume, S. Zhang, K. Yi, Z. Wu, P. Wu, The rice CK2 kinase regulates
697 trafficking of phosphate transporters in response to phosphate levels, *The Plant Cell*, 27 (2015)
698 711-723.
699 [85] M.K. Tarrant, H.-S. Rho, Z. Xie, Y.L. Jiang, C. Gross, J.C. Culhane, G. Yan, J. Qian, Y.
700 Ichikawa, T. Matsuoka, N. Zachara, F.A. Etzkorn, G.W. Hart, J.S. Jeong, S. Blackshaw, H.
701 Zhu, P.A. Cole, Regulation of CK2 by phosphorylation and O-GlcNAcylation revealed by
702 semisynthesis, *Nature Chemical Biology*, 8 (2012) 262-265.
703

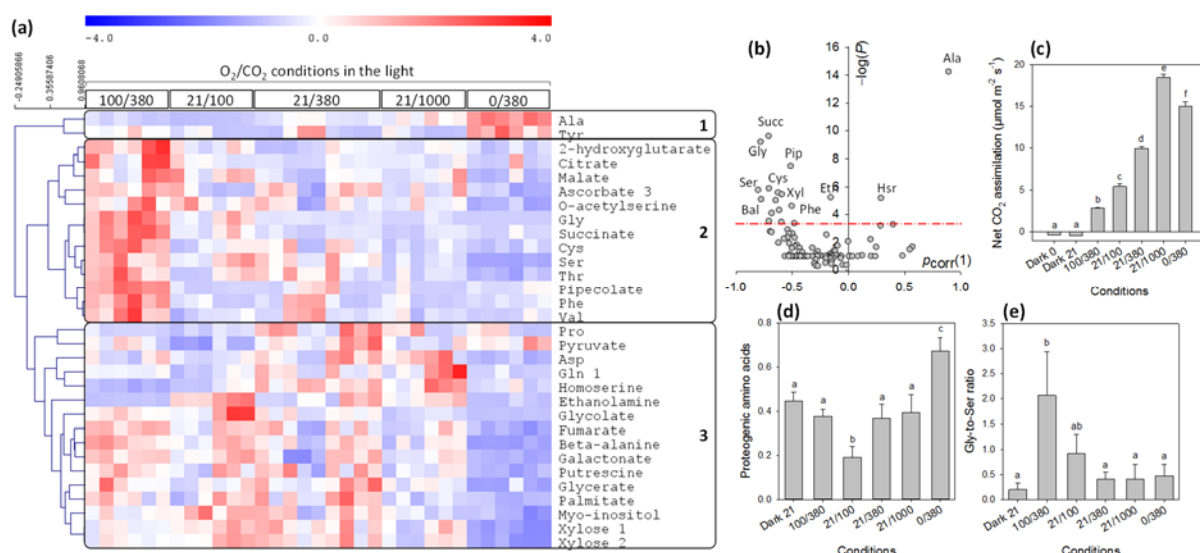


Fig. 1. Metabolism of Arabidopsis rosettes under different O₂/CO₂ conditions. (a) Heat map showing metabolites (from GC-MS metabolomics profiling) significantly different between O₂/CO₂ conditions in the light using a one-way ANOVA ($P < 0.01$). Hierarchical clustering (Pearson correlation) is shown on left. Metabolite contents (mean-centered values) are shown with colors (color scale on top). Since most metabolites change considerably in darkness, dark conditions are not included in the heat map so as to show metabolites only significantly affected by photosynthetic conditions per se. Main groups identified by clustering are boxed and labelled with numbers. **For each O₂/CO₂ condition, the $n = 6$ samples are shown**, except under standard conditions (21% O₂-380 $\mu\text{mol mol}^{-1}$ CO₂) where $n = 9$. (b) Volcano plot showing most discriminating metabolites, with $-\log(P\text{-value})$ (y axis) and the loading in the OPLS analysis ($p_{\text{corr}}(1)$; x axis). The red dash-dotted line stands for the Bonferroni threshold. (c) Photosynthesis (net CO₂ assimilation) measured by gas exchange. (d) Total content in proteogenic amino acids (relative to internal standard, ribitol, and normalized to DW). (e) Glycine-to-serine ratio. In (a), numbers on right refer to groups (metabolite clusters) discussed in main text. Numbers associated with metabolite names refer to distinct derivatives (analytes) of the same metabolite. In (c-e), letters stand for statistical classes ($P < 0.05$). In (c), the rate of CO₂ evolution (respiration) in darkness is also indicated (either in 0% or 21% O₂) and in (d-e), values obtained in the dark at 21% O₂ are also shown. **Abbreviations:** Bal, β -alanine; Cys, cysteine; Etn, ethanolamine; Gly, glycine; Hsr, homoserine; Phe, phenylalanine; Pip, pipecolate; Pro, proline; Ser, serine; Succ, succinate; Thr, threonine; Val, valine; Xyl, xylose. A magnified version of this figure is available as Fig. S7.

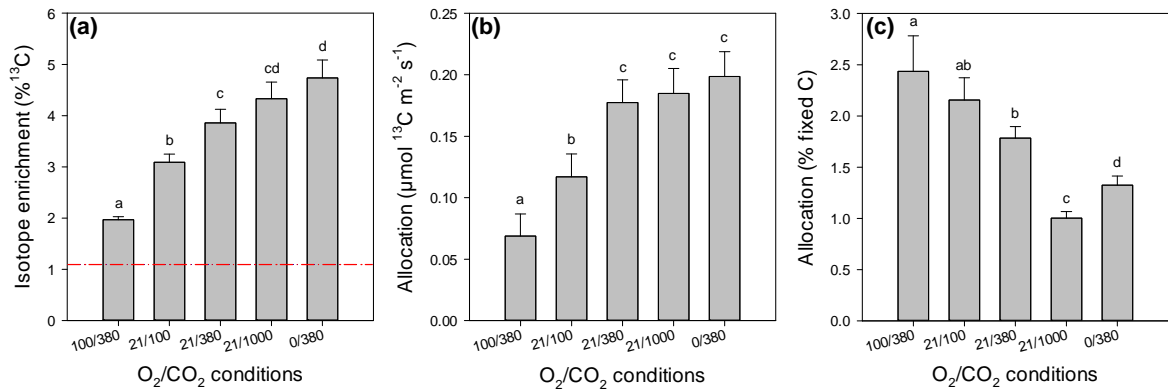


Fig. 2. Carbon allocation to protein synthesis determined by ¹³CO₂ labelling in the light. (a) Isotope enrichment (% ¹³C) in proteins, measured by isotope ratio mass spectrometry (EA-IRMS) on purified proteins. (b) Allocation of ¹³C to protein (apparent flux to protein synthesis). (c) Allocation expressed in percentage of photosynthesis (¹³C partition to protein synthesis) calculated from (b) and photosynthesis (given in Fig. 1). In (a), the red dash-dotted line stands for ¹³C natural abundance (enrichment in proteins measured after gas exchange carried out with ordinary CO₂). In (b-c), the contribution of natural abundance has been subtracted. Letters stand for statistical classes ($P < 0.05$).

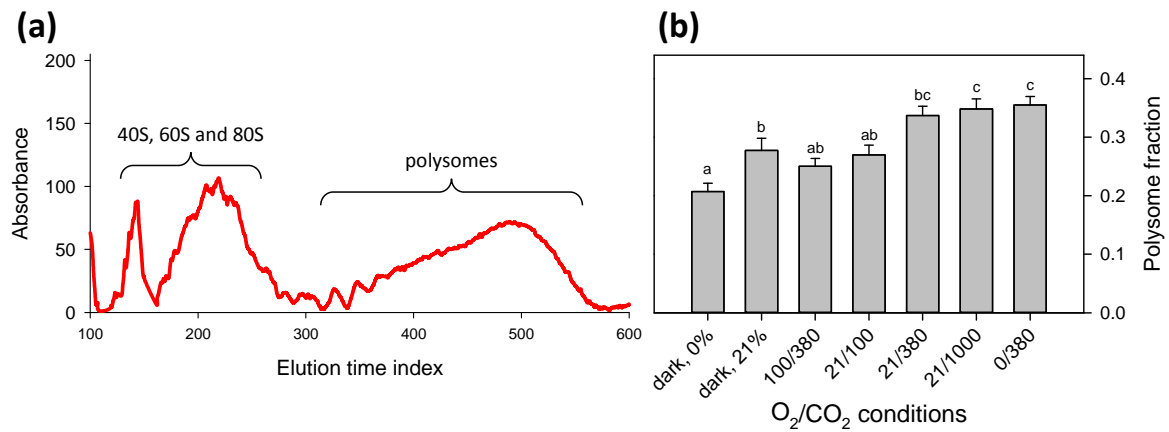


Fig. 3. Polysome abundance determined with gradient separation and absorbance at 260 nm. (a) Typical background-subtracted absorbance profile (standard conditions, 21% O₂, 380 $\mu\text{mol mol}^{-1}$ CO₂) showing the oscillating peak region on right corresponding to polysomes (legend after [68]). (b) Quantitation of polysome fraction from background-subtracted traces, in % of total signal. In (b), letters stand for statistical classes ($P < 0.05$). Note that (b) also shows results obtained in darkness at either 0% or 21% O₂, with a significant down-regulating effect of anoxia on polysome abundance.

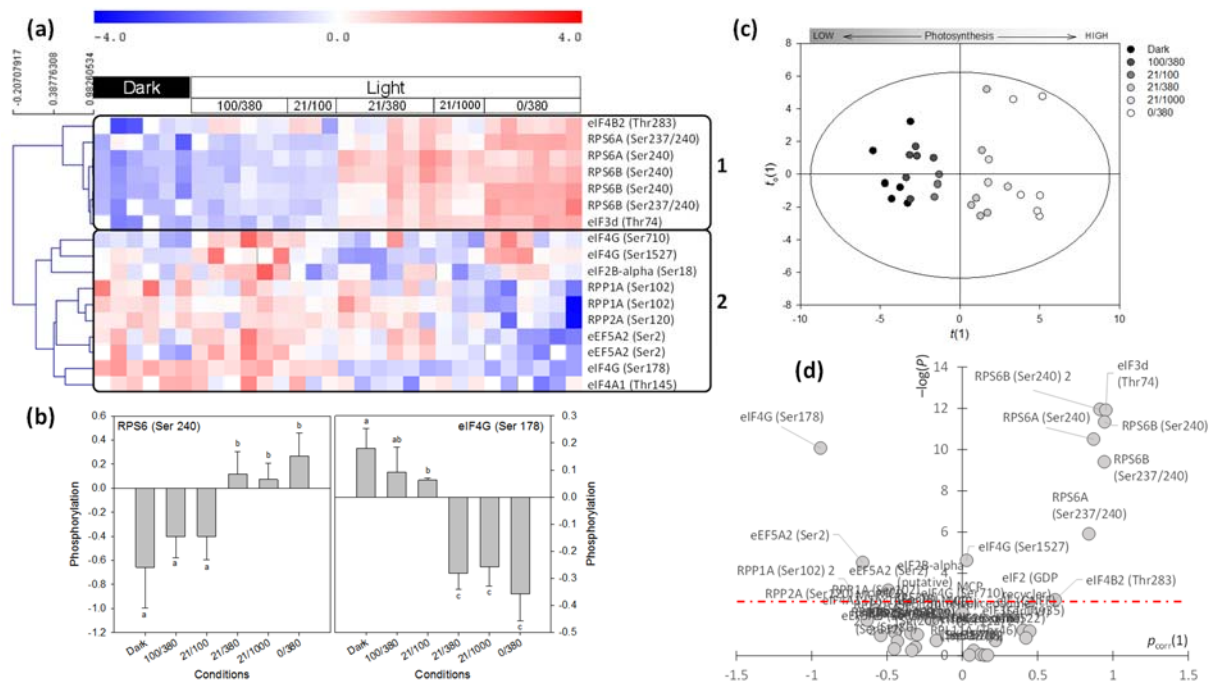


Fig. 4. Phosphorylation pattern of molecular actors involved in translation. (a) Heat map showing significant phosphosites with $P < 0.05$, with a hierarchical clustering on left (Pearson correlation). Main groups found by clustering are boxed and labelled 1 and 2. When phosphosite identifiers appear several times (e.g. RPS6A Ser240), it refers to analytically different phosphopeptides. “Dark” refers to darkness at 21% O_2 . In the light, O_2/CO_2 conditions are recalled (%/ppm). (b) Lookup of average phosphorylation at Ser 204 in RPS6A and RPS6B (left) and Ser 178 in eIF4G (right). Letters stand for statistical classes ($P < 0.05$). (c) Score plot of the OPLS multivariate analysis using photosynthetic conditions as a quantitative variable (aligned along the x axis). (d) Volcano plot combining univariate ($-\log(P)$ from ANOVA) and multivariate (loading $p_{\text{corr}}(1)$ from the OPLS) analyses showing most significant phosphosites. Red dash-dotted line, Bonferroni threshold ($P = 0.0014$). A magnified version of this figure is available as Fig. S8.

Table 1. List of phosphopeptides found here, associated with protein synthesis. The column “New” indicates phosphosites that are absent from (Boex-Fontvieille et al. 2014) and references therein, and the database Phosphat 4.0 (<http://phosphat.uni-hohenheim.de/>). “Occ.” Indicates when a phosphopeptide was found to be occasionally detected, that is, missing across more than 20% of the samples. Statistics reported in Fig. 4 only used non-occasional phosphopeptides, that is, with less than 20% missing values. In the column “Comments”, the term “common to” means that the phosphopeptides (with the same sequence) can also be found in other isoforms of the protein, but disambiguation could be done here. The nomenclature for eEFs and eIFs is after [12], except for the ubiquitin-binding elongation factor eEF1B (AT5G53330) which is recognized as an elongation factor in TAIR but is not listed in [12] and is also referred to as a cell wall proline-rich protein in Protein Data Bank.

ATG number	Name	Phosphosite	Comments	New	Sequence	Occ.
Elongation factors (eEF)						
AT1G07920	eEF1-alpha	Thr82			FE(pT)TKYYCTVIDAPGHR	Yes
AT1G30230	eEF1B-beta	Thr91			ISGVSAEGSGVIVEGSAPITEEAVA(pT)PPAADSK	Yes
AT5G53330	eEF1B-related	Ser58	Ubiquitin-binding elongation factor		N(pS)SFQHNTSPSSGIGIR	Yes
AT1G69410	eEF5A3	Ser2			(pS)DDEHHFESSDAGASK	
AT1G26630	eEF5A2	Ser2			M(pS)DDEHHFEASESGASK	
		Ser2			(pS)DDEHHFEASESGASK	
Initiation factors (eIF)						
AT2G34970	eIF2B-epsilon	Thr522			DKLSEITQAIDDDD(pT)DDESVVPTSGELK	
AT1G48970	eIF2B-delta 2	Ser149		Yes	LSA(pS)LPNGGFDLTLAVR	
AT1G72340	eIF2B-alpha	Ser18			RSSN(pS)PPMADTTR	
		Ser18			SSN(pS)PPMADTTR	Yes
AT5G38640	eIF2B-delta 1	Ser126			SSVPVA(pS)SLPGIGMDSMAAAK	Yes
		Ser88			VAVAGAAAASAV(pS)PSSFSYSSR	Yes
		Thr230			A(pT)SQKNDVAVATGAAEK	Yes
		Ser108			DFPDGSTTA(pS)PGR	Yes
		Ser108			RDFPDGSTTA(pS)PGR	
		Ser69			LN(pS)SDTFPLR	Yes
AT5G25780	eIF3B2	Ser684	common to eIF3B1		QNLRDGEV(pS)DVEEDEYEAK	Yes
AT3G56150	eIF3C1	Tyr35			(pY)LQSGSEDDDDTDTKR	
		Ser38/40			YLQ(s)G(s)EDDDTDTKR	
AT4G20980	eIF3d	Thr74			NLSNPSARPN(pT)GSK	
AT3G13920	eIF4A1	Ser4			AG(pS)APEGTQFDAR	Yes
		Thr145	common to eIF4A2		VHACVGG(pT)SVR	
AT3G26400	eIF4B1	Ser237			(pS)STFGSSFGDSSGQEER	Yes
AT1G13020	eIF4B2	Thr283			KADTEVSE(pT)PTAVK	
AT3G60240	eIF4G	Ser178			TT(pS)APPNMDDQKR	
		Ser710			STEGSSHASSEISGS(pS)PQEK	
		Ser1527			QVLQGPSATVN(pS)PR	
AT2G24050	eIFiso4G2	Ser512		Yes	(pS)LSVNSR	Yes
AT1G77840	eIF5	Ser200			NH(pS)SDEDISPK	
		Ser200/201			NH(s)(s)DEDISPK	Yes

Other molecular actors

AT1G64790	ILA	Ser1887	ILITHYIA (activator of GCN2 and thus of eIF2)	ALLEGG(ps)DDEGASTEAAQGR	Yes
AT1G80930	MCP	Ser187	MIF4G domain-containing spliceosome subunit	VIADKP(ps)DEEDDR	
		Ser187		VIADKP(ps)DEEDDRQR	
		Ser80		RKET(ps)DDEELAR	
		Ser112		IEVD(ps)DGDGERR	
		Ser112		RIEVD(ps)DGDGER	
AT1G48920	NUC-L1	Ser163	Nuclear RNA binding protein L1 (ribosome synthesis)	ESSSEDDS(ps)SEDEPAKKPAAK	Yes
Ribosomal proteins					
AT3G58660	RPL10E	Ser6		TTAV(ps)PPPPQEQQLVHASQTSR	Yes
AT2G42740	RPL11A	Thr46	common to RPL11B, RPL11C and RPL11D	VLEQLSGQ(pT)PVFSK	
AT5G23900	RPL13D	Thr138		AGDS(pT)PEELANATQVQGDYMPIASVK	Yes
AT3G09200	RPP0B	Ser305		VEEKEE(ps)DEEDYGGDFGLFDEE	Yes
AT3G11250	RPP0C	Ser308		KEE(ps)DEEDYEGGFGLFDEE	Yes
		Ser308		VEEKKEE(ps)DEEDYEGGFGLFDEE	Yes
AT1G01100	RPP1A	Ser102	common to RPP1B and RPP1C	KDEPAEE(ps)DGD LGFGLFD	
		Ser102	common to RPP1B and RPP1C	KKDEPAEE(ps)DGD LGFGLFD	
AT2G27720	RPP2A	Ser120	common to RPP2B and RPP2D	EKKKEEKEE(ps)DDDMGFSLFE	Yes
		Ser120	common to RPP2B and RPP2D	KEEKEE(ps)DDDMGFSLFE	
AT2G27710	RPP2B	Ser120	common to RPP2A and RPP2D	EKKKEEKEE(ps)DDDMGFSLFE	Yes
		Ser120	common to RPP2A and RPP2D	KEEKEE(ps)DDDMGFSLFE	
		Ser77		LASVPSGGGGVAVA(ps)ATSGGGGGGASAAESK	Yes
AT5G57290	RPP3B	Ser90	common to RPP3A	KEE(ps)EEEEGDFGFDLFG	Yes
		Ser90	common to RPP3A	KKEE(ps)EEEEGDFGFDLFG	Yes
AT2G45710	RPS27A	Ser29	common to RPS27B and RPS27C	LVQ(ps)PNSFFMDVK	
AT2G41840	RPS2C	Ser273		AL(ps)TSKPDVVEDQA	Yes
AT3G04840	RPS3Aa	Ser236		LMDVHGDY(ps)AEDVGVK	
AT4G31700	RPS6A	Ser240		L(ps)SAAAKPSVTA	Yes
		Ser240		SRL(ps)SAAAKPSVTA	
		Ser237/240		(s)RL(s)SAAAKPSVTA	
AT5G10360	RPS6B	Ser240		L(ps)SAPAKPVAA	
		Ser240		SRL(ps)SAPAKPVAA	
		Ser237/240		(s)RL(s)SAPAKPVAA	
AT1G74970	RPS9 (chloroplastic)	Ser47/Thr51		RA(s)LSITA(t)VSAPPEEEEEIVLKK	Yes
AT5G15200	RPS9B	Ser68		DLLTLDEK(ps)PR	Yes

Supplementary Material

Article title: Cytoplasmic protein synthesis increases with photosynthesis via the stimulation of translation initiation

Authors: Tcherkez G, Carroll A, Abadie C, Mainguet S, Davanture M, and Zivy M

Supplementary methods: polysome analysis

Liquid nitrogen-frozen rosette tissues weighing ~3-5g were ground to a fine powder in 20 mL polypropylene scintillation vials at approximately -40°C in a Cryogenic Grinder/Dispenser robotic system (Labman) by vigorous shaking with five ethanol-washed 8mm stainless steel ball bearings for 1 minute (two 30 s pulses with a 30 s pause in between). Weighed aliquots of the resulting tissue powder (100 ± 15 mg) were automatically dispensed into 1.4 mL screw cap polypropylene tubes (FluidX P/N 66-52330-Z6) and kept frozen until analysis. Polysomes were extracted after [69]. Extraction was performed with 500 μL of polysome extraction buffer (200 mM Tris pH 9.0; 200 mM KCl, 25 mM EGTA pH 8.3; 36 mM MgCl_2 ; 0.8% v/v β -mercaptoethanol; 50 $\mu\text{g mL}^{-1}$ each of cycloheximide and chloramphenicol; 1% (v/v) each of Triton X-100, Brij-35, Tween-40, NP-40; 2% (v/v) polyoxyethylene-10-tridecyl-ether and 1% sodium deoxycholate) was added to the frozen tissue powder aliquot and mixed by inversion. To prepare negative control gradients, tissues from 380 ppm $\text{CO}_2/21\%$ O_2 treatments were extracted with extraction buffer containing 50 mM EDTA (and analysed on gradients containing 100 mM EDTA) instead of MgCl_2 . Samples were incubated on ice for 3 min before being centrifuged through Qiagen Qias shredder spin columns at 16,000 g for 1 min to remove debris. Portions of the flow-throughs (250 μL) were loaded onto 14 mL 20-50% (w/v) sucrose continuous density gradients prepared in 14 x 89 mm ultracentrifuge tubes (Beckman Coulter P/N 331372) using a Gradient Master 108 device (Biocomp) according to manufacturer's directions. Gradients were prepared just prior to use, kept at 4°C and loaded in a 4°C cold room. The loaded gradients were centrifuged at 360,000 g for 135 minutes at 4°C in a SW41 rotor in a Beckman Coulter ultracentrifuge. The gradients were then analysed by absorbance of 260 nm wavelength light using a Foxy R1 density gradient analyser (Teledyne ISCO) according to manufacturer's directions. UV absorbance profiles were plotted onto chart recorder paper (Chart speed = 60 cm h^{-1} , Sensitivity = 0.5, Peak separator = OFF, Noise filter = 1.5). These plots were then scanned at 600 dpi using a desktop document scanner. The vertical pixel heights of the plotted signals relative to the y-axis scale were detected on the basis of pixel hue and saturation of the red plot lines, sampled at regular 5-pixel intervals (gradient indices) and exported into raw [gradient index \times relative absorbance signal intensity] spreadsheet tables using an in-house C++ software package based on OpenCV (<https://opencv.org>) and Qt (<https://www.qt.io>). The top of the gradient (volume index = 0) was defined as the point where the downward slope of the intense chlorophyll absorbance peak crossed the top of the y-axis scale. A baseline correction was applied to each signal profile by subtracting the average signal intensity of two negative control gradients at each index from the signal intensity at the corresponding index of the gradient being corrected. Corrected values slightly below zero were set to zero. The translational activity factor (polysome relative abundance) was then calculated for each gradient by dividing the integrated signal area in the polysomal region of the gradient (index 200 to 600) by the sum of the areas under both the polysome region and the upper ribosomal/monosomal region (index 0 to 600).

Supplementary Text

• Phosphorylation sites in eIFs found here

In general, the higher translational activity in the light compared to the dark is assumed to stem from an increased phosphorylation of eIFs 3 and 4B and inhibited by phosphorylation of eIF2 α [11, 16]. We show here experimentally that phosphorylation of eIF4B2 and eIF3d correlate with that of RPS6 and translation activity and anti-correlates with eIF4G (Figs. 3 and 4). The phosphorylation sites found here have been previously identified in *Arabidopsis* (Table 1) and here they may behave as molecular switches to control translation. In particular, while eIF4G phosphosites at Ser 710 and 1527 did not correlate linearly with photosynthesis, Ser 178 phosphorylation was clearly anti-correlated to photosynthesis (Fig. 4b). This phosphosite has also been shown to be affected by the light-to-dark transition [11]. The specific role of phosphorylation at this site is presently unclear and eIF4G possesses multiple phosphorylation sites with contrasting effects. In yeast and mammals, phosphorylation of eIF4G near the C-terminus has been shown to stimulate translation by promoting the formation of the eIF4F complex and subsequent binding of 5' RNA cap (for a review, see [70]). By contrast, upstream phosphorylation in the RS domain of the protein (such as that found in eIFiso4G2 at Ser 512 here; Table 1) inhibits eIF4E binding and translation [71]. Here, the observed phosphosite at Ser 178 is situated in the mRNA-binding region [72] and thus phosphorylation likely impedes formation of the eIF4F complex and thus translation initiation.

By contrast, translation stimulation appears to be accompanied by increased phosphorylation of eIF4B2 and eIF3d (Fig. 4). Although eIF4B in plants is less characterized than in mammals, it is essential for preinitiation complex formation and mRNA recruitment. Its phosphorylation, which has been demonstrated in vitro with CK2 as a kinase [24], might play a significant role in promoting the helicase activity of eIF4A and mRNA binding [73]. Interestingly, the sequence of this protein varies considerably and the site found here (Thr 283) is not present in some non-Brassicaceae species. eIFs of the eIF3 group are known to be phosphorylated, including eIF3c, eIF3h and eIF3i that have been shown to be phosphorylated by CK2 [24], S6 kinase/mTOR [74] and brassinosteroid kinase [75], respectively. Also, eIF3d that been shown to be more phosphorylated at Thr 74 in planta in the light compared to the dark [11]. In Mammals, it has been shown that eIF3d allows translation of specific mRNAs independently of the complex eIF4F [76]. It is currently unknown if such a mechanism also takes place in plants (and *Arabidopsis* eIF3d possesses only 42% identity with human eIF3d).

• Possible involvement of SnRK1

Arabidopsis SnRK1 has been found to be inhibited by a variety of sugar phosphates (reviewed in [77, 78] and oxidation of the Cys 200 residue of AKIN10 (SnRK1 α 1) [79]. SnRK1 has also been found to participate in controlling translation by phosphorylating eIF4E and eIFiso4E [20]. That is, it is plausible that the effect on translation seen here was the combined effect of SnRK1 inhibition when gross photosynthesis increases (increased production of sugars) and photorespiration decreases (lower H₂O₂ production in photorespiratory cycle). That said, while this mechanism provides a probable explanation for RPS6, it cannot be at the origin of eIFs phosphorylation changes with photosynthesis. In fact, most phosphorylation motifs found here are of the CK2 (x-(**pS/T**)-D/E-D/E/x-D/E) or cyclin-dependent kinase (CDK) type (x-(**pS/T**)-P-x-x-R/K/x) (Table 1), suggesting an important role of these kinases. In particular, CK2-mediated phosphorylation of several plant eIFs has been found to take place, at least in vitro [24, 25, 80]. However, mechanisms regulating CK2 activity are presently unclear. It is generally believed that **plant** CK2 is a housekeeping, constitutively expressed kinase [81] the α/β isoform composition of which changes in response to environmental conditions – typically with mineral nutrition [82-84]. Also, both phosphorylation and N-acetyl glucosamination of CK2 have been found

in human cells, with differential effects on activity [85] but the way such post-translational modifications are affected by environmental conditions is, to our knowledge, unknown. It should also be noted that ethylene signaling may represent another link between photosynthetic conditions and CDK-mediated phosphorylation, since ethylene production and perception have both been found to correlate with the photorespiration rate (reviewed in [31]).

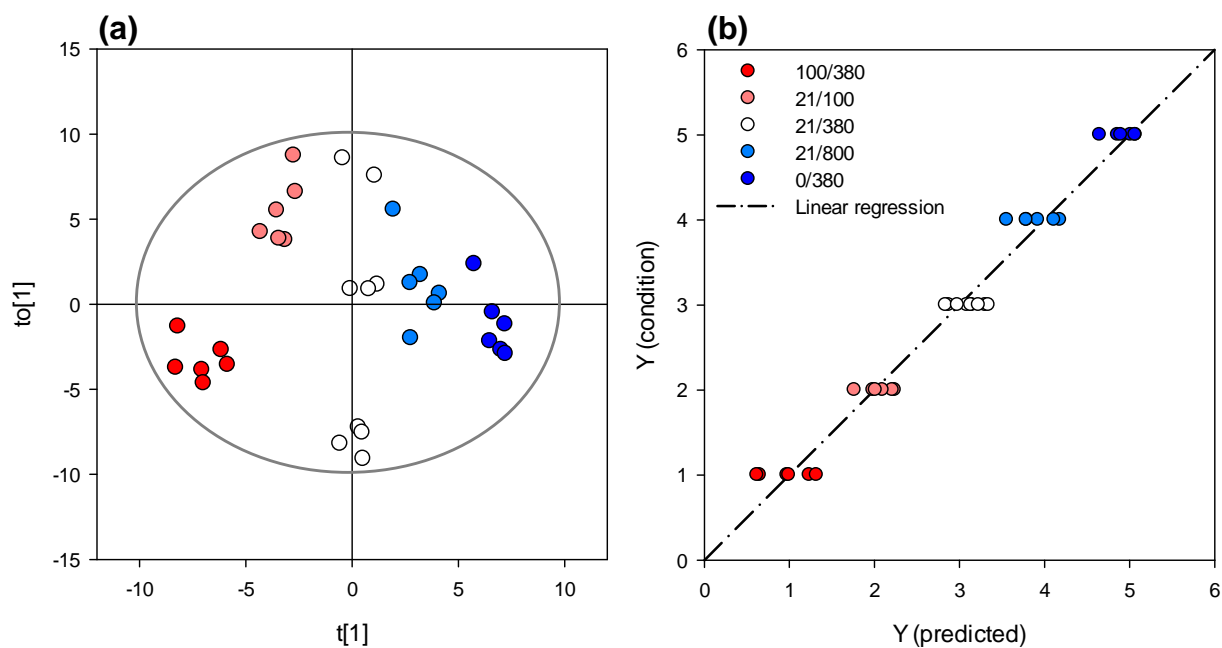


Fig. S1. Output of the OPLS analysis of metabolomics data, using O₂:CO₂ conditions as a quantitative Y variable. (a) Score plot showing samples in the first component space. (b) Relationship between predicted and observed Y variable showing the very good agreement of the OPLS model. Note the natural variability of metabolic contents along axis 2 (orthogonal component 1), not due to O₂:CO₂ conditions. In (a), the grey line represents the Hostelling's 95% confidence ellipse.

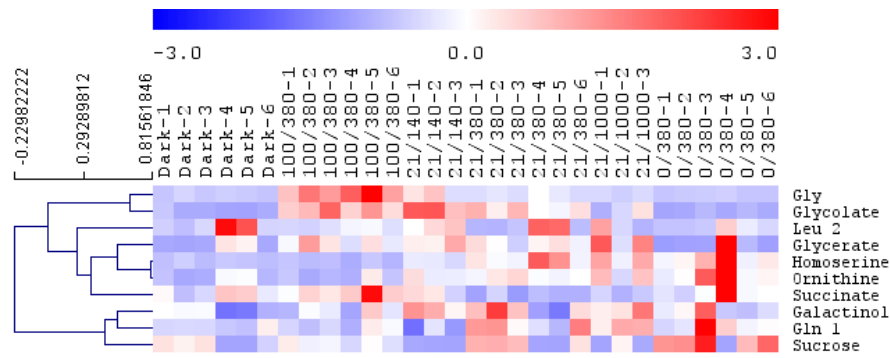


Fig. S2. Metabolites that are significantly different in the dark compared to the light (at 21% O₂), with $P < 0.05$. Hierarchical clustering (Pearson's correlation) is shown on left. As expected, photorespiratory metabolites glycine and glycolate are represented, as well as photosynthetic products sucrose and galactinol. Note however the rather variable content in sucrose in the dark so that sucrose is not significant at the 1% level (Fig. S2). CO₂/O₂ conditions are shown on top.

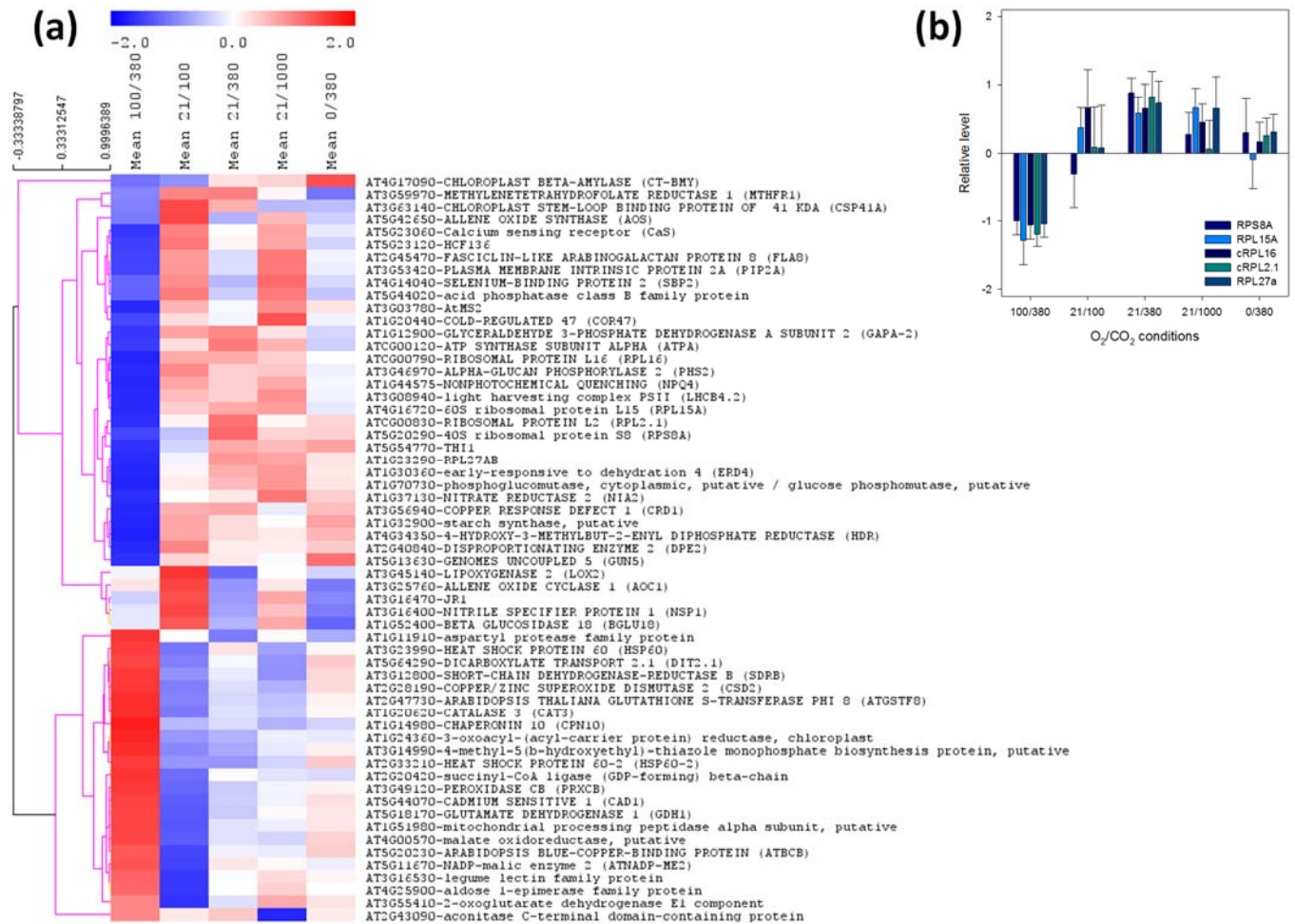


Fig. S3. Significant changes in total proteins: (a) summary heat map showing only significant (< 0.05 , one-way ANOVA, with Benjamini-Hochberg correction) proteins, with a hierarchical clustering (Pearson correlation) on left; (b) Detailed pattern of ribosomal proteins that are amongst significant proteins in panel (a). Note that none of the proteins listed in Table 1 is found here, showing that changes in phosphopeptide abundance is not due to changes in total protein quantity. In (b), the letter “c” is added in front of names when the associated gene is chloroplast-encoded.

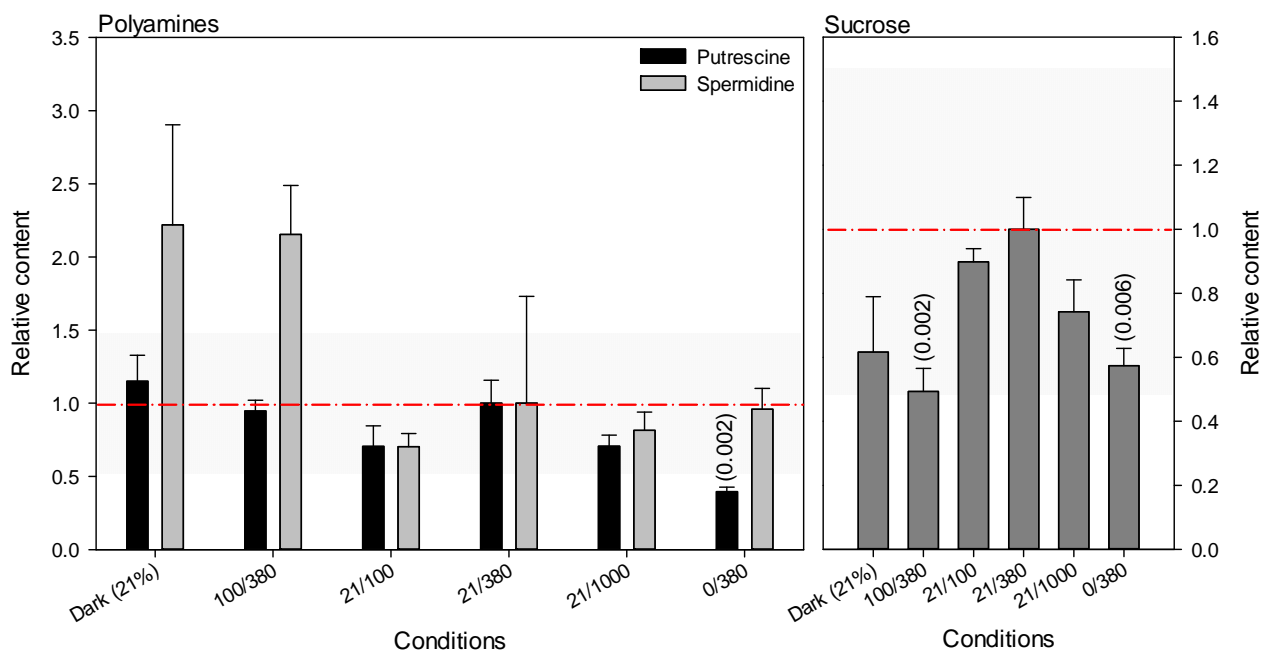


Fig. S4. Content in polyamines and sucrose in *Arabidopsis* rosettes under different O₂/CO₂ condition, from GC-MS profiling analyses. Content are expressed relative to standard gaseous conditions (21% O₂, 380 μmol mol⁻¹ CO₂). When significant in paired test (Student-Welsh, *P* < 0.01) with comparison to standard conditions, the *P*-value is shown between parentheses. Red line: standard content; shaded area: ±50% region. Note that due to substantial variability between plants, there is no significant variation in spermidine.

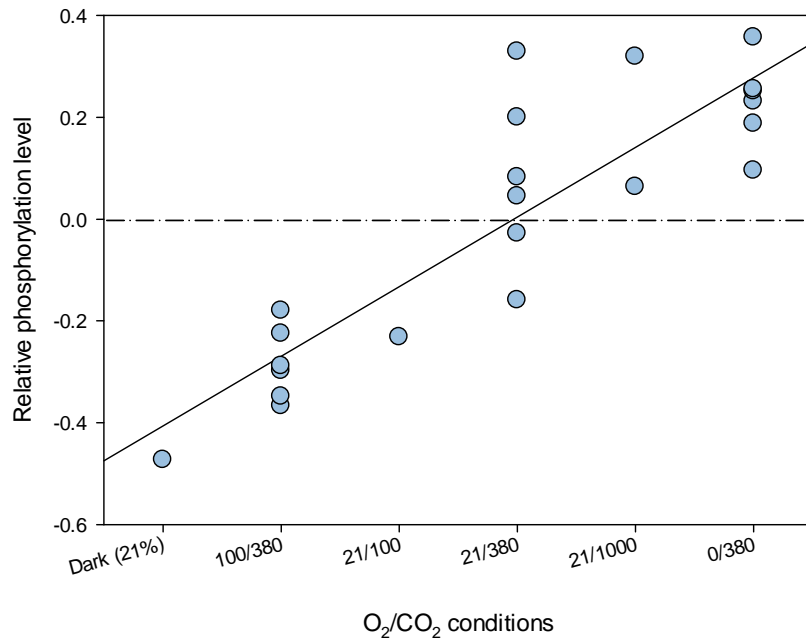


Fig. S5. Relative phosphopeptide abundance associated with nucleolin-like 1 (NUC-L1) (phosphosite Ser 163; phosphopeptide ESSSEDDS(pS)SEDEPAKKPAAK). Note missing data particularly in the dark and at low CO₂ (only one replicate in each), showing that this phosphopeptide is only occasionally detected. However, available data suggest a positive relationship with photosynthesis (linear regression, solid line).

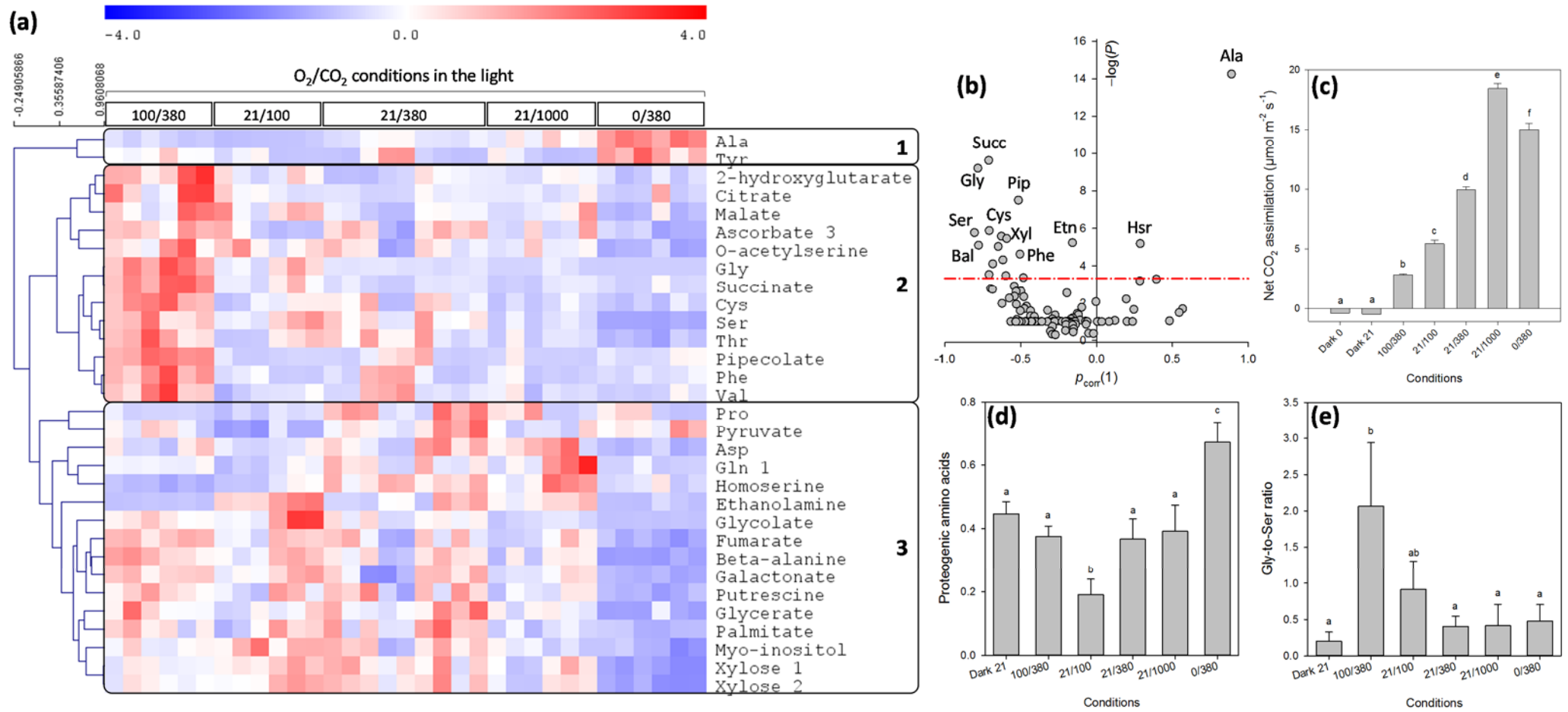


Fig. S7. Magnified version of Fig. 1.

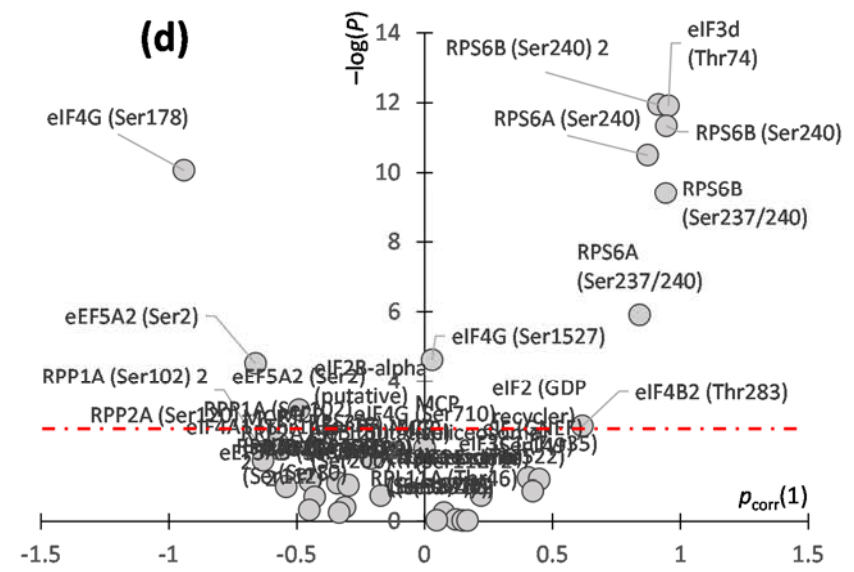
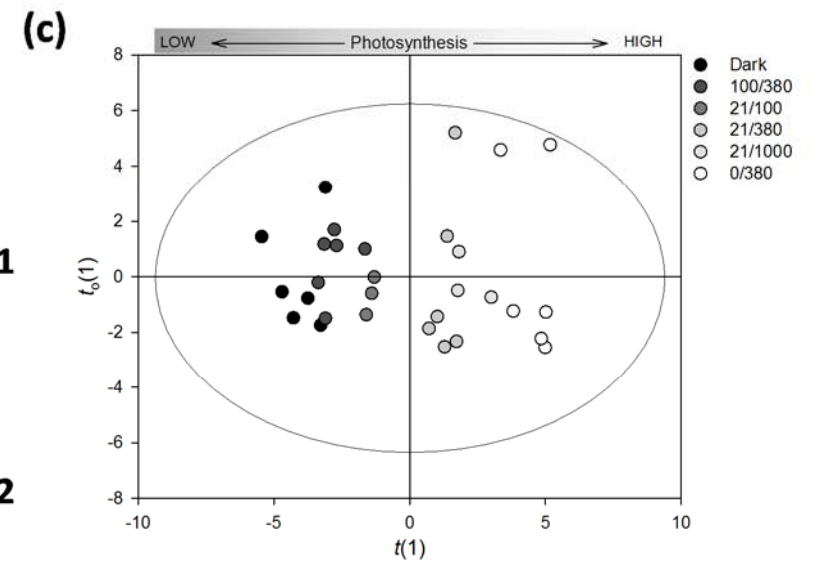
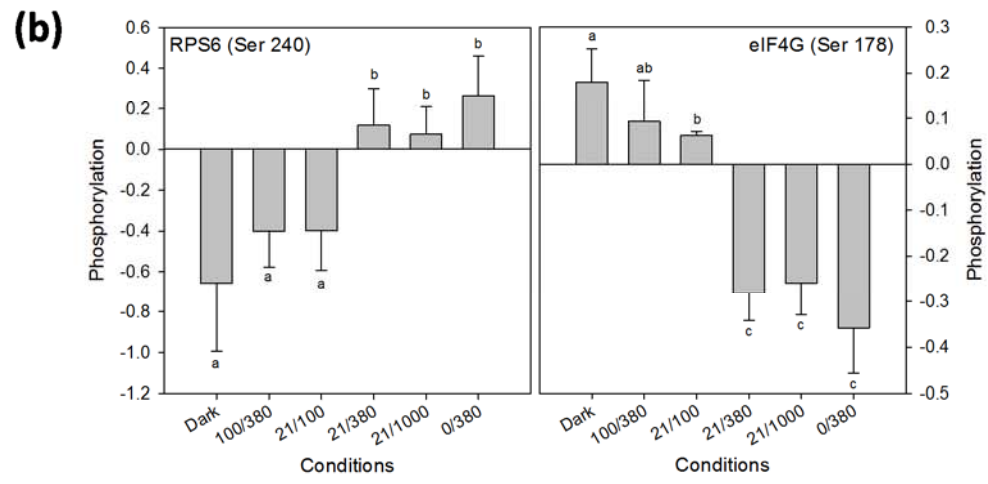
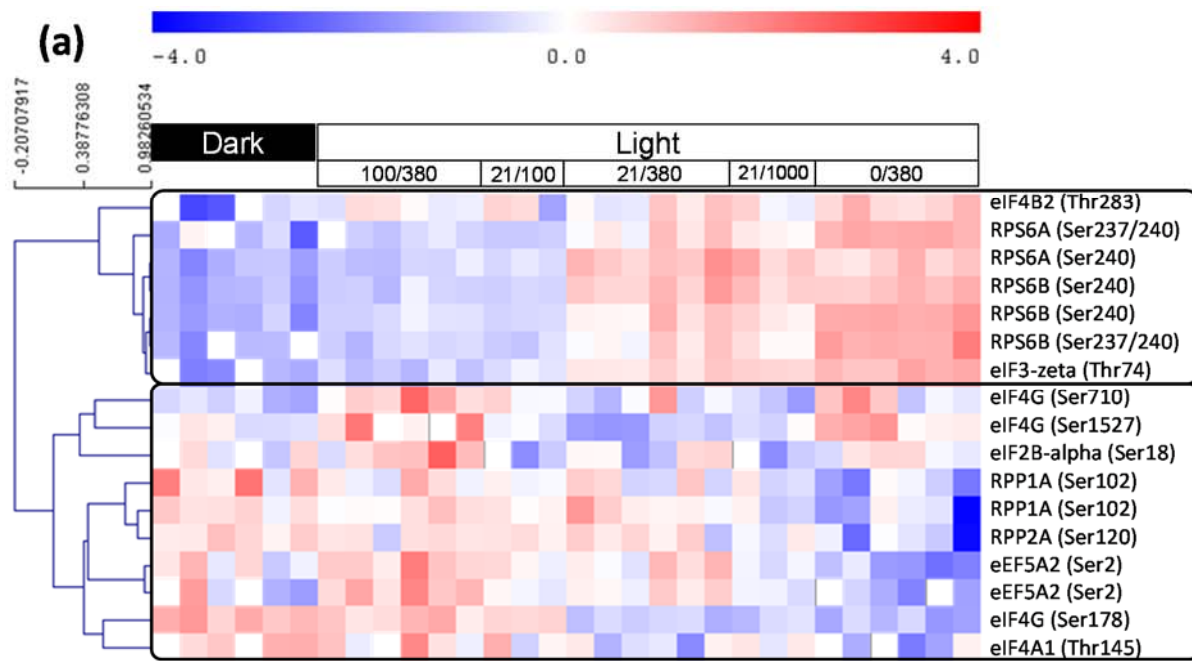


Fig. S8. Magnified version of Fig. 4.